2

EGG-APO-10944
November 1993

Idaho National Engineering Laboratory

Managed by the U.S. Department of Energy

Four Beam Interferometer Manual

Operating Instructions for the INEL Diffraction Moiré Interferometer

RECEIVED
MAY 09 1994
OSTI

EG&G Idaho

Work performed under DOE Contract No. DE-AC07-76ID01570

DISTRIBUTION OF THIS DOCUMENT IS UNLIMITED

EGG-APO-10944

FOUR BEAM INTERFEROMETER MANUAL

OPERATING INSTRUCTIONS FOR THE INEL DIFFRACTION MOIRÉ INTERFEROMETER

VANCE A. DEASON

Published November 1993

IDAHO NATIONAL ENGINEERING LAB (INEL)
EG&G IDAHO, INC.
IDAHO FALLS ID 83415

Prepared for the
U.S. Department of Energy
Under DOE Idaho Operations Office
Contract # DE-AC07-76ID01570

MASTER

DISTRIBUTION OF THIS DOCUMENT IS UNLIMITED

ABSTRACT

Moiré interferometry is an interferometric method for measuring changes of in-plane geometry. It is essentially insensitive to out-of-plane topography or changes in that topography. Changes in geometry are referenced to a particular moment in time when the moiré sensor, a diffraction grating, was attached to the specimen. Distortions experienced by the specimen prior to that time are not directly detectable, although they may be inferred from specimen behavior or condition.

In its most common form, moiré interferometry is not well suited to large (> 50 mm square), curved (< 300 mm diameter) or high temperature (> 200 C) regions. However, various efforts have been made to handle each of these conditions. In general, the moiré process is most straightforward for flat, 25 mm diameter regions of coverage and room temperature. Much smaller or larger regions require more specialized optics, which can become very expensive.

This report will discuss various aspects of moiré interferometry. In particular, a new four beam (bi-axial) interferometer is described in detail. Issues involved in safety, assembly, calibration and use are fully explained.

NOTICE: The moiré interferometer described in this document is currently available for licensing from EG&G Idaho, Inc. For more information, please contact:

Vance Deason
EG&G Idaho, Inc.
PO Box 1625, MS 2211
Idaho Falls, ID 83415
(208)526-2501
Fax: -2814
email: vac@inel.gov

ACKNOWLEDGMENTS

There have been many people involved in the development of the INEL moiré interferometers and the associated data system. Among these I would like to especially thank the following:

Prof. Dan Post (VPI and SU) for his support and encouragement.

Dr. J.S. Epstein for advice.

Michael B. Ward for creative solutions to mechanical design problems.

Jim Lee for electronic design and development.

Gordon Lassahn for the development of the original phase shifting algorithms and FORTRAN code.

Jeff Lassahn for converting the FORTRAN code to the C language during a fruitful summer internship.

Paul Taylor for moving the data acquisition and reduction code to the Windows environment, and for spending many hours of personal time resolving problems and adding features.

Funding: there have been many sources of funding for various aspects of the INEL moiré effort. In particular I would like to thank the following:

Office of Arms Control for the initial code development and for early design work on the hand held interferometer, the first phase shifted moiré system at the INEL.

BES for support of several moiré efforts.

USAF for partial development of the four beam interferometer and of the Microsoft Windows based data system.

CONTENTS

Abstract i
Acknowledgments ii
Table of Contents iii
Introduction 1
Safety 2
General Principles 3
Initial Assembly and Alignment 5
Experimental Alignment and Operation 10
Data Reduction: General Overview 16
The INEL FRINGE© * Program 19
Appendix A: Operation of the Automated Data System 21
Appendix B: File Formats Used in FRINGE© 27
Appendix C: Evaluations 29
Appendix D: Publications of Interest 32
Appendix E: Moire Detailed Description of Data Analysis Process 35

* Copyright Pending

INTRODUCTION

THE INEL MOIRÉ INTERFEROMETRY EFFORT

In 1985, Dr. J.S. Epstein joined our staff. He had been a graduate student at Virginia Polytechnic and State University where he was trained in moiré interferometry techniques by Prof. Post and others. He and I then embarked on an effort to develop a moiré capability at the INEL and to extend the technique in certain directions of interest to us. In particular, I wanted to reduce the size and complexity of the equipment and simplify the operating and data reduction procedures so less highly trained technicians could operate the systems.

Among the improvements I have included in our interferometers are:

1. Use of optical fiber components: this greatly reduced the complexity and size of the system without a significant change in cost.

2. Use of phase shifting techniques: this permits automated data reduction and greatly improves the resolution of the technique.

3. Development of compact systems: this opens up the possibility of fieldable units for NDT examinations of working components for cumulative strain.

Our most recent interferometers include full biaxial data acquisition, automated data reduction, compactness, simplicity of operation and quick setup. All relative to earlier systems, of course. Moiré interferometry is still a fairly labor intensive process, but the quality and quantity of data it affords the user normally outweigh the negative aspects. In particular, the need for applying a sensor (diffraction grating) is often quoted as a negative aspect of the technique. However, for those used to using strain gauges, this requirement will not seem troublesome. In fact, applying a moiré sensor is scarcely more involved than applying a strain gauge. It should also be remembered that competitive techniques such as holographic interferometry are not without their own problems, particularly in the area of data reduction.

SAFETY

The degree of hazard of the moiré interferometer depends on the intensity of the output laser beams. This in turn depends on the power of the system laser, system losses and on the beam diameter of the output beams. The initial laser power, I, is reduced by losses in the laser to fiber coupler, in the fibers and in the fiber optic beam splitters. Further losses and reductions in beam intensity occur as the laser beams exit the fibers and expand to fill (or over fill) the collimation lenses. The focal length and diameter of these lenses affects the total power and the power density of the output beam.

Longer focal length collimating lenses imply lower power density and larger lens diameters imply more efficient collection of the expanding laser beam from the fibers. In general, diverging laser beams are less hazardous to the eye than collimated beams due to the focusing properties of the human eye. There is usually little chance of skin damage with the types of lasers used in moiré interferometry. It is possible for a moiré interferometer to be made into a class 1 laser system, if laser intensity and beam diameters are properly chosen. In general however, this will not be the case.

It is recommended that all laser operations meet at least the ANSI laser safety standards as embodied in ANSI-Z136.1-1986. Other regulations may apply, depending on where the system is being used. At minimum, one should avoid looking into the direct laser beam, whether from the laser or from one of the collimating lenses. It is also possible for one of the diffracted beams from the specimen diffraction grating to be intense enough to damage the eye, although these beams are rarely more than 20 % of the initial laser power due to various losses and the effects of low diffraction efficiency of the grating. We sometimes use a 4 watt Argon ion laser as a source, and any beam from such a system is potentially capable of causing retinal damage.

A further safety concern arises with the use of certain gratings, where multiple beams are formed. These beams often occur at unexpected angles due to periodic structures in the grating oriented at angles other than the principal horizontal or vertical grooves. The zero order diffracted beams (corresponding to ordinary reflection) are particularly bright and should be blocked from accidental view. For grating groove densities less than 1000 lines per mm, higher diffraction beams may be produced, with more beams occurring the coarser the grating. These beams are difficult to remember, and should be blocked whenever they exceed the damage threshold.

Finally, for crossed gratings (simultaneous horizontal and vertical grooves), there will be extra beams diffracted by periodic structures occurring 45 degrees to the principal grooves. These periodic structures are caused by the intersections of the horizontal and vertical grooves. One must develop the habit of remaining constantly aware of all of these possible beams if they are capable of eye damage.

GENERAL PRINCIPLES OF OPERATION

The best source of information and guidance on the basic concepts and techniques of diffraction moiré consists of the body of papers written by Post and others at Virginia Tech. An especially complete introduction is the chapter on Moiré Interferometry by Post in the SEM "Handbook of Experimental Mechanics," edited by A. Kobayashi. I highly recommend that beginners and more experienced users alike consult this source. Dr. Post is also writing a more complete volume devoted exclusively to the subject which should be published in 1994.

In diffraction moiré interferometry, one can consider the interference as a purely optical phenomena where a diffraction grating is used to combine two independent laser beams so as to interfere. Alternately, one can use a more mechanistic approach and describe the interference as the mixing of bar patterns to create traditional moiré fringes. It can be shown that the two approaches lead to similar mathematical descriptions. However, I feel it is always important to remember that, physically, we have true optical interference of wave fronts, not the mechanical mixing of patterns, as in classical or coarse moiré techniques. In the latter case, a pattern is applied to a specimen and then compared with a physical master pattern with moiré fringes mapping out differences between the two patterns.

The moiré interferometer is essentially a device which generates one or more pairs of mutually coherent collimated laser beams and directs them so that they each illuminate the same region of a diffraction grating at precise and equal incident angles. The grating interacts with each of these beams to generate (diffract) a secondary beam which exits the grating perpendicular to its surface. The secondary beams are collected by a lens and imaged by a integral CCD video camera or by a film camera. Various configurations of the optical and mechanical elements are possible and size, weight and shape can be modified to conform to particular requirements.

As with any form of interferometry, diffraction moiré relies on the comparison of optical wave fronts. All diffraction moiré interferometers create these wave fronts through the interaction of a pair of mutually coherent beams with a diffraction grating. Each laser beam produces one or more diffracted beams. In the usual configuration, the +1 diffraction order from one beam leaves the grating coincident with the -1 beam from the other incident beam. These beams therefore interfere, with the optical wave front aberrated locally by a particular point on the grating. Each wave front (due to each incident beam) is aberrated in an equal but opposite manner so the total combined effect is twice that for each wave front singly.

It can be shown that if a grating is replicated into a thin adhesive layer on the surface of a specimen, then as the specimen is distorted, so is the grating, thus

aberrating the diffracted wave fronts. Local distortions produce local aberrations in the wave fronts. The relationship between the interference fringes and the surface displacement U_x due to stress is $U_x = (1/f)N_x$, where the grooves of the grating are assumed to be aligned perpendicular to the x direction on the specimen. N_x is the number of full and partial fringes crossed by a line drawn between a reference point and the observation point. A similar equation holds for Y displacements.

Note that in moiré interferometry, only displacements normal to the grating groove direction are measured. Crossed gratings provide simultaneous sensitivity to both X and Y displacements. The specific shape and orientation of the interference fringes is determined partly by factors other than the grating orientation. These fringes may be quite complex and are, in effect, a contour map of in-plane displacement in a direction perpendicular to the grating grooves.

INITIAL ASSEMBLY AND ALIGNMENT OF THE INEL FOUR BEAM INTERFEROMETER

This section is not intended as a complete assembly procedure. Instead, it is intended as a fairly detailed overview of the assembly and alignment process. This will serve as a guide for those with maintenance responsibilities for the INEL interferometer.

A. ASSEMBLE CASE

1. Prepare sides, base and top of case.

2. Tack weld sides and base to form rigid case assembly.

3. Drill holes in top cover to match tapped holes at top of side walls.

B. INSTALL FIBER COUPLER ASSEMBLY AND PROTECTIVE SHEATHS

1. Lay out exit fibers to full length along table.

2. Lay protective sheath along side fibers
   * Be sure to apply significant tension to sheath to remove all slack so as to avoid later stress to fiber if sheath is extended.

3. Allow for short loop of fiber inside case (about 4 inches). Mark sheath shorter by this distance.

4. Cut sheath with abrasive cut-off wheel.

5. There is usually a sharp point of steel left at the end of the sheath. Bend this out, cut it off and buff the ends of the sheath on a Scotch Bright wheel to soften all edges. This is important to avoid abrasion to the fiber.

6. Install fiber coupler assembly in final case, pass output fibers through individual exit ports and install each output fiber in its own sheath.

7. Apply epoxy to the end of the sheath and to the strain relief clamp and install and clamp the sheath to the case.

8. Apply epoxy to the other end of the sheath and insert it into the brass fiber terminator.

9. If desired, install protective sheath in a similar manner on input fiber (from laser). This is not necessary if the laser is internal to the interferometer case and the fiber is not exposed to abuse.

10. Inspect ends of all fiber sheaths. If desired, extra epoxy can be used to cover any exposed sheath edges and further protect the fibers from abrasion. Be sure that epoxy does not reduce sheath diameter and prevent passage of the fiber connector.

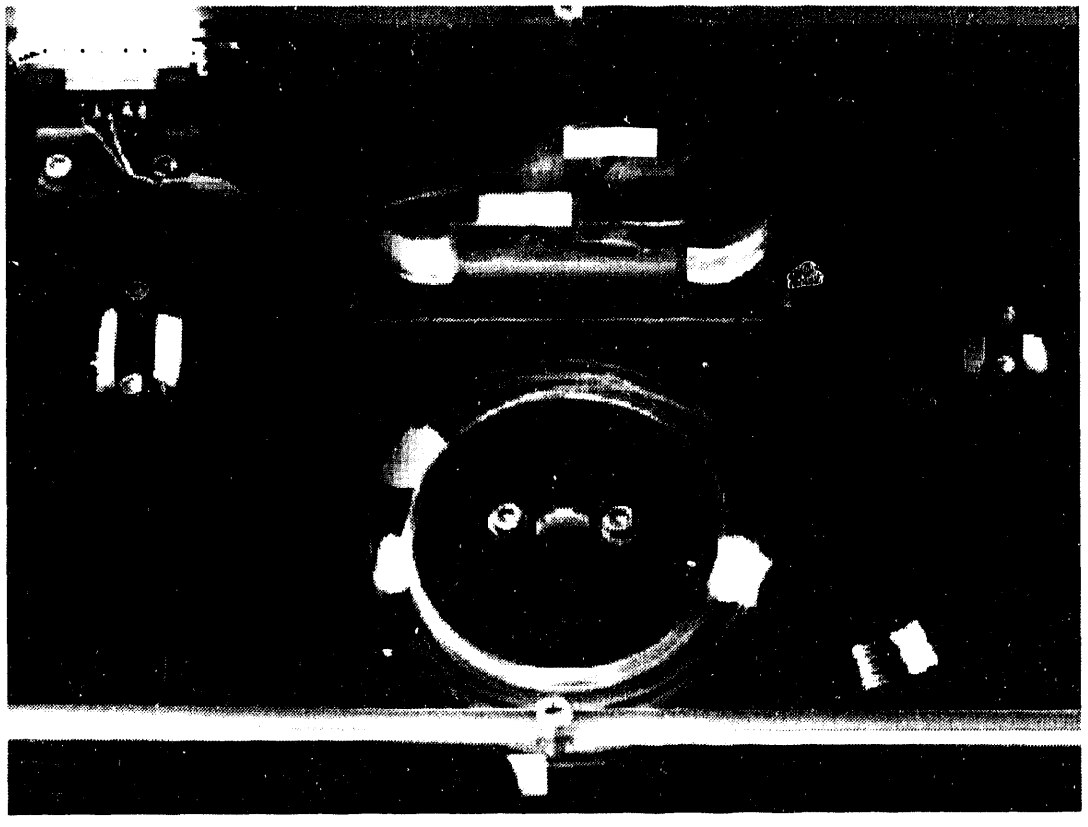

Figure 1. Canadian Instrumentation
Fiber Couplers and Phase Shifter

C. INSTALL AND ALIGN LASER TO FIBER COUPLER

<u>Safety</u>: This system contains a 10 mW Class IIIb HeNe. Such lasers are capable of causing significant eye injury in the form of retinal burns. Careful design of the INEL moiré interferometer has reduced the potential for exposure to hazardous beam intensities to a minimum. Unless the interferometer is modified by the user, the only place where the user can access the full beam intensity is between the microscope objective and the fiber tip in the laser-to-fiber coupler. This beam is highly converging, which is considered to be less damaging than collimated beams.

<u>Laser Intensity:</u> It is always best to reduce the laser intensity to the minimum practical level during all alignment procedures and to avoid direct viewing of any of the beams formed by this system. The laser intensity is controlled by

adjusting the fine alignment knob of the laser to fiber coupler (either of the pair of knobs closest to the laser).

1. Install laser and laser power supply and make all electrical connections. Install beam expander on laser. This improves coupling efficiency into the fiber.

2. Install the fiber terminator and mount the laser coupler in the case. Align the polarization of the fiber with that of the laser (the fiber polarization may have been marked by the manufacturer, or may have to be determined by the user. The laser polarization is usually marked).

3. Align fiber so as to couple maximum laser power into fiber.

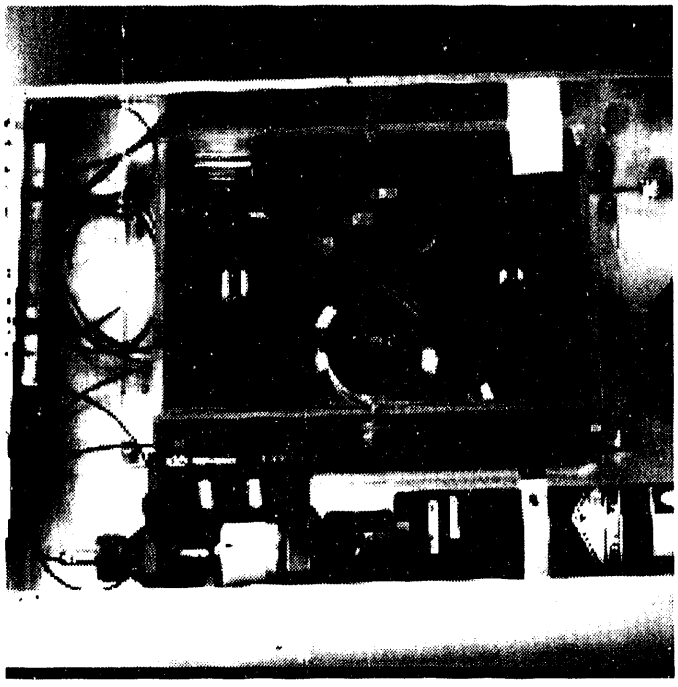

Figure 2. Laser and Laser-to-Fiber Coupler

D. INSTALL OUTPUT FIBER IN INTERFEROMETER ASSEMBLY

The fiber output has two orientation factors: beam angle and beam polarization. These are typically independent alignment requirements.

1. Mount gimbal lens holder on the rotary base plate. Install lens to fiber assembly in the gimbal and tighten the holding ring. Install the Nikon lens mount on the lens to fiber assembly and attach the gimbal with rotary plate to the rail carriage. Do this for each of the four gimbals.

2. Each fiber is equipped with an FC connector polished at 8 degrees to reduce back reflection . The output beam therefore leaves the connector at an angle of about 4 degrees due to the prism effect of the slanted end. Insert each fiber into one of the brass fiber terminators. Insert the terminator into the eccentric cylinder and the cylinder into the rear of the collimation lens assembly.

3. Adjust the collimation lens focus to slightly less than infinity. This allows one to use the focus knob to make slight corrections to collimation.

4. Push the brass fiber terminator all the way into the eccentric cylinder and tighten the set screw (being sure to use a tapped hole which is located over the brass wall of the terminator).

    a. Rotate the brass fiber terminator until the polarization is vertical (check with piece of polarizing film).
    b. Rotate the eccentric holder while maintaining the polarization direction until the output beam is concentric with the collimation lens (coaxial). Closing the iris to restrict beam passage to the center of the lens may help in determining this. Adjust the eccentric holder until the central part of the beam passed by the iris is brightest.
    c. Lock all relevant set screws. Note that a ring and pin fixture holds the eccentric cylinder orientation while focus and polarization adjustments are made.

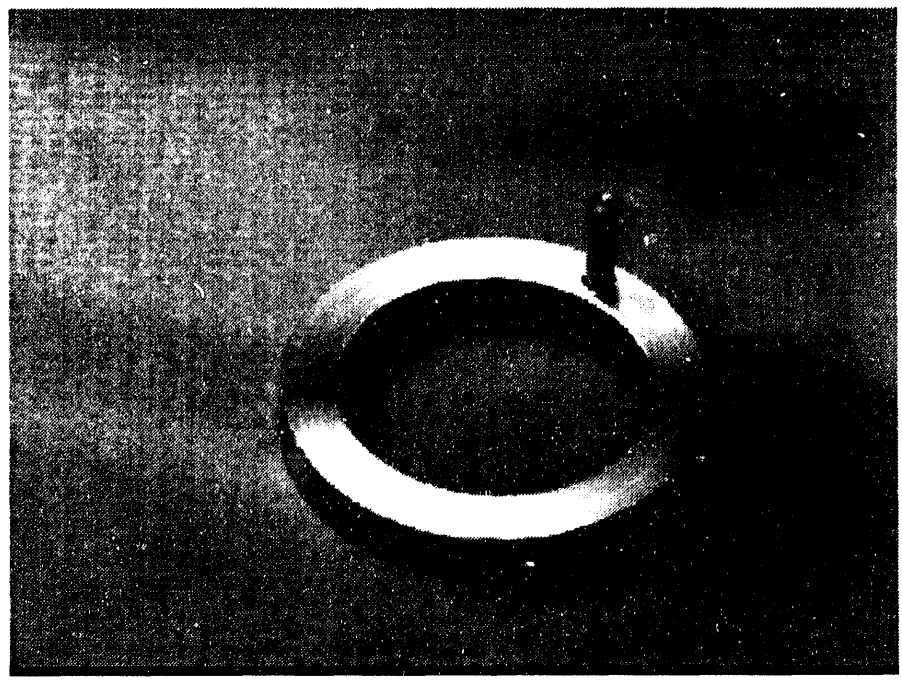

Figure 3. Ring and Pin Assembly

5. Using the shear wedge collimation tester, adjust the eccentric in and out until the collimation is optimized (the fringes are aligned with the line on the viewing screen).

EXPERIMENTAL ALIGNMENT AND OPERATION

The INEL moiré interferometers come in various forms and are either two beam (uniaxial data) or four beam (biaxial data). While the compactness and ease of use of the basic INEL design is retained in most cases, the biaxial systems are inherently more complex to align and use. This is due to the extra degrees of freedom possessed by such systems. Research interferometers are typically more complex than those designed for field use where fewer degrees of freedom are desirable.

For four beam systems, it is usually easiest to select one axis, the horizontal or U axis, for example, and align that axis as one would a uniaxial system. The vertical beams are then aligned with each other and with the horizontal beams. This alignment process is not difficult, but does require one to follow a set procedure.

A. General Alignment

This falls under the category of "good housekeeping". It is important, from time to time, to check all of the positions and coarse adjustments of the interferometer. This is especially true if a critical test is to be conducted.

1. Center all support rods on the central cube. Adjust the collimator carriages to be equidistant from the central support. Note that one set of rails is positioned farther from the specimen than the other. Carriages on the far rails must be slightly farther out on the rails if the beams are to intersect at the same specimen plane as beams from the other axis. This extra spacing depends on the beam angle (or grating spacing). One can calculate the extra spacing as follows:

$$b = c \tan \theta$$

where b is the additional spacing required for the carriage, c is the offset between rail sets and θ is the beam half angle

For example, if we take the preset angles (for 300, 600 and 1200 lines per mm specimen gratings), then we have the following relationships:

Specimen Grating (lines/mm)	Beam Half Angle	Additional Carriage Spacing (mm)
300	10.94	2.15
600	22.31	4.56
1200	49.41	12.98

2. Check that the polarization of all four beams is in the same direction (usually vertical) and that the beams are collimated. Check that the collimated beams are coaxial with the optical axis of the collimation lens. If not, see the assembly instructions and correct the problem.

3. Return gimbals to zero position (facing the central hub): this must be done periodically to simplify alignment. Rotate all collimation lenses to the center so that lens pairs point at each other (note: some lenses are too large to permit this step. In this case, adjust the gimbals to their central angles). Turn on the laser and adjust the gimbal mounts of opposing collimation lenses so that the beams are coaxial. Hold a piece of typing paper in front of each lens and note the relative position of the two beams. Closing the iris to reduce beam diameter may help locate the center of the beam. One can use a mirror to view the opposing beams location on the iris itself and adjust the other gimbal to center the spot.

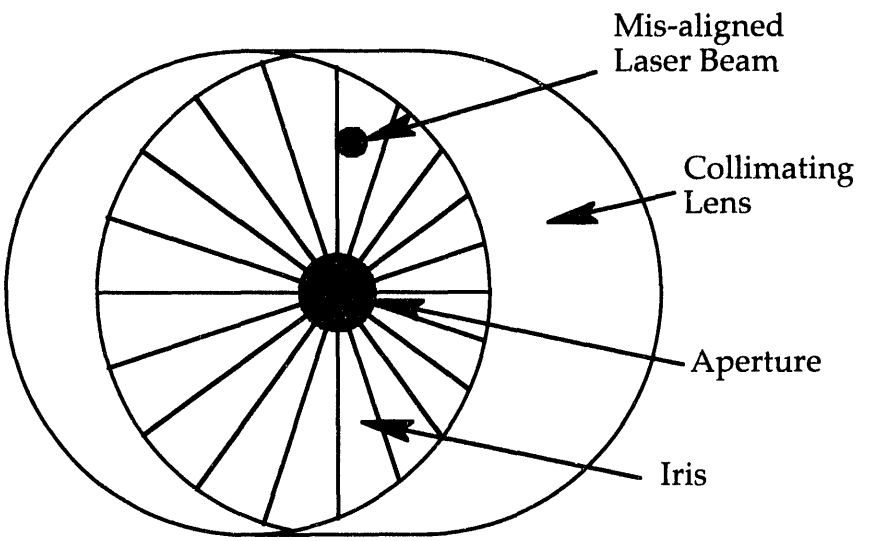

While observing the laser spot, adjust the gimbals of the opposite lens to place the spot inside the aperture of the iris (fully stopped down).

4. Rotate each of the gimbal mounts to the correct angle for the specimen grating being used. Holes in the rotary base plate allow one to set the angle for 300, 600 and 1200 line per mm specimen gratings when using a HeNe laser. Lock the gimbal in position. Other positions must be set manually using a protractor or other aid. The finer gratings (>300 l/mm) have the smallest angle relative to the carriage rods. Note that this is only a coarse alignment aid.

5. Check to see that the four beams intersect at the proper distance (at the intended specimen location). If not, adjust the lateral position of the carriages on the support rods until the beams intersect at the desired specimen position.

B. Specimen Alignment

1. Coarse Alignment

The specimen grating or a trial grating is placed at the intersection of the beams and specimen or interferometer is rotated so that the grating is perpendicular to the central axis of the interferometer. One can check this by first turning off the laser and then sighting down the central tube of the system and seeing that the reflection of the eye in the specimen grating is well centered.

Alternately, a small HeNe laser could be installed on the system axis and the beam directed at the center of the desired region of the grating. The main reflected beam (zero order diffracted beam) should return down the incident beam path and enter the laser aperture. The four first order beams (two vertical and two horizontal) should strike the centers of the collimating lenses if the system is properly aligned. Small errors will be corrected later, but it is helpful to do a good job of alignment at this stage.

Once the specimen and interferometer are roughly aligned, one can do the final alignment by any of several methods, or a combination of methods. Turn on the main laser. For safety, it is best to turn the laser beam intensity down to as low a level as is practical. To do this, mis-align the laser to fiber coupler by turning one of the screws nearest the laser (the fine adjustment). One of these can be turned by a screw driver through a hole in the side of the interferometer case. This saves opening the lid and exposing the delicate fibers to possible damage from dropped tools.

2. Fine Alignment

Alignment Methods: A diffraction moiré interferometer is said to be aligned when the fringe pattern caused by the interference of the two first order beams is as coarse as possible. Ideally this will be an "infinite" fringe (a fringe broader than the field of view), but in practice, various aberrations of lens and grating will introduce some minimum fringe set which must be accepted as the null alignment. Normally, one can subtract out this initial fringe pattern by recording it for future reference.

If one arrives at this stage (after completing the coarse alignments described in the preceding section) without seeing any fringes in the diffracted beams

when they are allowed to fall on a piece of white paper, then one must use other alignment methods.

Remember: the purpose of alignment is to bring the pair(s) of first order diffracted beams produced by the pair(s) of incident beams into colinearity. When this happens, the interference fringes described by the interference equation are as broad (coarse) as possible.

A popular method for alignment is to place a long focal length lens, say 500 mm, in the diffracted (data) beams and hold a card at the focal point of the lens. One will see two bright spots (or four for a biaxial system with all four beams open) on the paper if the system is mis-aligned and one superimposed spot if the system is aligned. It is usually less confusing to block off two of the beams.

One must adjust the gimbals until both (or all four) spots lie on the same point. If the lens is removed at this point, one can usually see fringes on the paper. If not, then a magnifying lens will usually show them. One continues to adjust the gimbals until the fringes are as coarse as possible.

One can also let the beams fall on a ground glass and look at the fringes with a magnifier from the back side. This is usually less awkward. Be sure the laser power level is below the damage level for the retina.

If the laser power is very low, one can put a video camera in the diffracted (data) beams , close all of the collimator lens irises and observe the cluster of light spots (focused laser beams) on the monitor. Remember that focused laser beams can be very bright and can damage the video camera just as they can the eye. The INEL interferometer is capable of complete control over the output beam intensity without any loss in optical alignment or beam quality.

By adjusting the gimbals, one brings all of the spots into coincidence. If the irises are now opened, one will see fringes which can be further nulled, if necessary.

C. Other Tricks for Alignment:

1. When one is near a good null, one can see faint "ghost fringes" directly on the surface of the specimen. These are visible due to variations in scattered light from the grating surface and are caused by beam intensity variations caused by constructive and destructive interference. These should be nulled.

2. Place a white card in the diffracted beams and put a fine object such as a pen point in the beam some distance from the card. If one sees two shadows of the pen on the card, then the beams are mis-aligned and the shadows must be brought into coincidence by adjusting the gimbals.

3. A video image or an image projected on a card by a lens will usually show some small defects on the grating: dust, scratches, fiducial marks, etc. Misalignment causes double images of these small objects. Adjust the gimbals until the images coincide, at which time fringes usually appear.

D. General Considerations for Alignment

It is important that one exercise considerable discipline in alignment of a four beam interferometer. Make sure that all four collimation gimbal mounts are centered before going on to other steps. Position the gimbal base at the proper angle for the grating being used. Choose one beam of one axis as the principle beam, say the right hand horizontal beam (Figure 1). Close all irises to the minimum size (maximum f/No). Adjust this beam so that it intersects the center of the subject grating and the first order beam passes down the center of the main support tube. A front and back disc on this tube with small centered holes can aid in this step. Small errors in this step are not serious.

A small alignment laser whose beam is coaxial with the central tube of the interferometer can also be used for alignment. The zero order beam from the specimen grating should retrace the data beam path, while the first orders should enter the center of each collimation beam and pass through the small iris opening. (Figure 2). The interferometer has lateral and rotational adjustments to help in this step. Avoid using the gimbal micrometers at this stage.

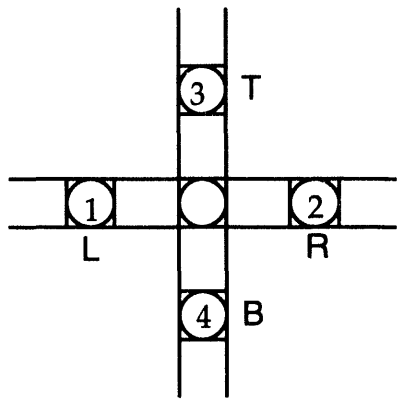

Figure 1. Suggested alignment order.

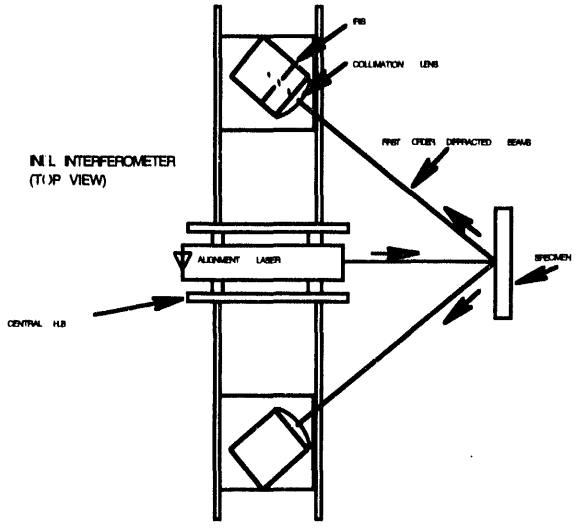

Figure 2. Use of a laser for alignment of the interferometer

Now adjust the other (left) beam of this first pair. Adjust the carriage position so that the beam falls on the center of the grating and the first order beam is approximately collinear with the right hand first order beam. Once the right hand beam is set, it becomes the reference beam, and no further adjustments should be made to it. Bring the left hand beam into alignment with the right using one of the alignment methods mentioned earlier. When the interference fringes are as broad as possible, cover the left hand beam and open one of the vertical beams, say the top beam. Adjust this beam as you did the left beam to bring it into alignment with the right hand beam. Shutter the top beam and open the bottom, then repeat to align this final beam with the right hand beam.

All four beams are now aligned so that their first order diffracted beams from the specimen are collinear with interferometric accuracy. Any two of the beams will interfere to produce usable data. Horizontal beams give U displacement fields, vertical give V. Furthermore, when the phase shifter is operating, all of the data will be phase shifted (it is necessary when combining one horizontal and one vertical beam to be sure that only one of the beams is phase shifted).

DATA REDUCTION: GENERAL OVERVIEW

There are many ways in which diffraction moiré data can be recorded and analyzed. Some of these ways can be very time consuming and tedious due to the quantity of data available in a single moiré interferogram. Traditionally, the fringe patterns were recorded on photographic film, processed, printed and manually reduced. This latter process involved digitizing the center lines of each fringe, fitting this data with a suitable mesh and then interpolating interior points. Often, the user simply picked a few points of interest, estimated their relative fringe numbers and then calculated the displacements at those few points. One would essentially use the moiré fringe pattern to decide the best place to measure the displacement. This was marginally better than using strain gauges at each point, but didn't provide time varying data, as the strain gauges can.

Various automated fringe tracing techniques have been developed, with various degrees of success. In general, these techniques work best on very simple fringe patterns with very low noise. Several of these techniques have been commercialized by companies like Wyko, Zygo and Phase Shift Technologies, among many others. The main customers for these products have been the optics manufacturing and testing companies and little attention has been given to the needs of other users of interferometry. For this reason, we decided to develop our own data reduction technique with the emphasis being diffraction moiré interferometry. This technique relies on video images and phase shifting algorithms.

Phase Shifted Data Acquisition and Reduction

Phase shifting requires that the optical phase of one of the beams of an interferometer be shifted relative to the other. This is usually done by changing the optical path of one beam by a small amount (less than one micrometer) in three or more steps adding up to a total phase change of 2π. A video image of the fringe pattern after each phase shift is collected. Phase shifting algorithms have been developed at the INEL and elsewhere to use these multiple interferograms to evaluate the data and compute accurate phase and deformation maps of the grating and the underlying material.

While this is not the place for a full explanation of the technique of phase shifting interferometry, a brief explanation may be helpful. Interferometry consists of the comparison of two optical wave fronts. These wave fronts are characterized by wavelength, intensity, phase and propagation direction. Interferometry deals only with relative phase measurements.

One of the beams is termed the reference beam, and is usually made as perfect as possible, while the other beam is called the object beam and has been distorted

by some experimental process (such as reflection from a mirror or by passage through a distorting medium). When the two beams are mixed (superimposed), optical interference occurs (linear summation of the sinusoidal electric fields which constitute the light). The process of constructive and destructive interference creates light and dark regions known as fringes. The more distorted the object beam becomes, the more complex the fringe pattern will be.

Diffraction moiré interferometry differs from most other types of interferometry in that both interfering beams have been aberrated by diffraction from the same grating by the same but opposite amounts. Thus, when these beams are combined so as to interfere, twice as many fringes are formed (i.e. the sensitivity of the interferometer is doubled).

Analysis of very complex, arbitrary fringe patterns by the conventional fringe tracing techniques is time consuming and difficult to automate. Furthermore, such analysis provides data only at points lying along the center lines of the fringes. Phase shifting methods greatly reduce the difficulty of analyzing interferograms, provide values at more points on the 2 dimensional interferogram and are easier to automate.

Phase Shifting Algorithms

To evaluate the data at a single point (usually called a pixel) on the interferogram, one must solve for the optical phase at that point. One must then apply some physical interpretation to the phase to determine the magnitude of the corresponding process which caused that phase variation. One difficulty is that phase is an angular term derived from a trigonometric function and has therefore a 2π ambiguity. Conditions which cause the phase to vary by more than 2π over the area of the interferogram require further processing of the data to remove this ambiguity.

In phase shifting, one records 3 (or more) interferograms where the relative phase of the beams has been artificially altered in 2 (or more) steps, for a total phase shift of less than 2π The physical effect of this is that the fringes in the interferograms are translated in position. No distortion of the data is involved. A phase shift of 2π would visually restore the appearance of the interferogram: all of the fringes would be back in the "same" position (another example of the 2π ambiguity mentioned earlier).

It can be shown that one can evaluate the relative phase of the two beams at each pixel if the phase shifts are known. The process involves solving a set of three (or more) linear equations involving the pixel intensities and phase shifts. This computation is done at each pixel in turn without reference to neighboring pixels. This is in total contrast to fringe tracing techniques which require

complex image processing decisions to be made as to where the fringes are located.

Once the phase is computed at each pixel, one must resolve any 2π ambiguities which exist and, if desired, convert phase to physical or engineering units. For a typical digitized video interferogram, this process results in over 256,000 individual phase values, each corresponding to a unique location on the grating. In the INEL data reduction routines, this large data block is displayed as a video image where the phase values are presented as an 8 bit gray scale intensity and are superimposed on the outline of the grating. Thus, each phase value is directly associated with its physical point of origin on the specimen.

The resolution of the digitizer is nominally 1 part in 256 but the accuracy of the entire system is probably about 1 part in 100 or 3.6 degrees due to errors in the camera and digitizer. For a typical 1200 line/mm grating, this would imply that one could detect a distortion as small as 0.000003 mm (3 nanometers) distributed over several centimeters. Funding has not permitted us to fully evaluate what the practical limits of accuracy actually are. In any case, our primary desire in this development was to simplify and automate the data reduction. Any improvement in accuracy is a welcome bonus.

THE INEL FRINGE© PROGRAM

This code was originally developed to reduce data acquired by the INEL hand held interferometer. This interferometer is a uniaxial system designed to read diffractive ID tags. Since then the code has been expanded and moved from FORTRAN to C and from DOS to Windows 3.1. We may at some point develop a Macintosh version as well.

The code provides for data acquisition, storage, retrieval, reduction and display. All data is displayed as 8 bit images (depending on monitor capabilities) with a basic 512 x 512 pixel array. The images and reduced data can be viewed either on the computer monitor or an RS 170 video monitor, depending on hardware capabilities.

A full data set consists of three or more phase shifted fringe images, two shuttered images (an option explained later), a mask, a folded phase and an unfolded phase. More detailed information about the various images and data sets used in FRINGE© can be found in the Appendices.

1. Phase shifted fringe images: These are recorded images of the fringe pattern generated by the interferometer. A phase shift is introduced between each of the images.

2. Shuttered Images: This is an INEL innovation which provides additional information and allows one to remove more of the optical noise and directly compute the phase shift without prior knowledge. These data are collected by recording the first order diffracted beam produced by each beam when all of the other beams are shuttered. There are no fringes in this image, but information about variations in beam intensity due to laser properties or diffraction efficiency can be derived from these data.

3. Mask: This image (data set) contains all pixels (points) on the specimen which the code determined were invalid or which the operator specified were not to be analyzed.

4. Folded Phase: this image contains the calculated phase values for each valid pixel in the raw fringe data. The phase at a pixel is directly related to the relative displacement of that pixel (specimen distortion). The folded phase contains a 2π ambiguity which must be resolved by a process known as unfolding.

5. Unfolded Phase: this data set results from unfolding the folded phase and is the final data set produced by FRINGE©. Further data reduction, for instance conversion to displacement or computation of contours are left to other custom programs such as Spyglass for the Macintosh.

Viewing the Data

Any aspect of the data analysis stream is available for viewing either on the computer monitor or on a video monitor. Raw data are automatically stored as they are produced to avoid data loss. Calculation times are relatively short (a minute or so) if a fast 486 CPU is used.

Further processing of the data is left to the user. At the INEL, we often export the data to a Mac IIci where we view the data using Spyglass. Contours, slices, perspective views or other techniques for viewing the data offer qualitative insight into the specimen condition. The large quantity of data produced by the interferometer (250,000 pixels with a 16 bit deformation value at each pixel) requires fast computation to reduce data manipulation times to reasonable levels.

APPENDIX A:
OPERATION OF THE AUTOMATED DATA SYSTEM

The INEL automated interferometric data acquisition and reduction system, "FRINGE© ", consists of the following software and hardware components.

Hardware

1. CPU: 33 MHz 80486, ISA bus, super VGA video, 8 Mb memory

2. Data Translation DT-2853 512x512x8 bit video frame grab board

Software

1. MS DOS 5.0, MS Windows 3.1

2. INEL "FRINGE© " and associated auxiliary programs

3. Spyglass and Dicer for the Mac

Special considerations:

1. FRINGE© will not run well in less than 8 Mb RAM. Also, due to restrictions imposed by the DT-2853, total RAM, including the 512 Kb on the frame grabber must not exceed 16 Mb, with the frame grabber at the top of memory.

2. Data sets are large, so archival disk space is consumed rapidly. We recommend using a lossless compression program, such as PK-ZIP. A full five step data set can be compressed to fit onto one high density floppy.

OPERATING PROCEDURES FOR FRINGE©

1. Orient and align specimen and interferometer (see earlier sections of this manual). For best results, the laser should warm up for about 20 minutes and the interferometer should be on a floated table.

2. Block the beam pair not in use.

3. In Windows, double click on the FRINGE© Icon.

4. In FRINGE© , pull down the "Frame Grabber" menu and select "Pass Through Mode". This sends the video signal directly to the external video monitor.

5. Adjust the specimen, interferometer and video camera to provide the desired data.

6. From the "Frame Grabber" menu, select "Acquire". Acquire one frame (dimension or mask will do), return the display to pass through and adjust the external video monitor so the appearance of the fringes closely matches that of the computer monitor image. This helps reduce errors in adjusting laser intensity to the proper level by compensating roughly for monitor characteristics.

7. Adjust the laser intensity to provide nearly saturated whites. The actual level can be determined by acquiring another single image and using the cursor to determine the intensity levels in the white fringes. This should not exceed 254, but should be as large as possible to assure full range data.

8. Acquire and analyze a fringe set:

Method 1: operator assistance required

Begin the Process

a. In the "File" menu, select "New". If an older data set is in memory, a dialog box asks if you wish to delete the old data. "No" returns the user to the desktop where he can proceed to save the old data using the "File" menu. "Yes" deletes the old data and prepares the system for a new data set.

b. In the "Frame Grabber" menu, select "Acquire", then "Fringe Set". A dialog box appears. Choose the number of fringe images to acquire. At least 3, but no more than 15; actual RAM currently restricts this to about 8. Five fringe sets is a reasonable choice and provides some improvement in the data due to least squares procedures in the data reduction algorithms.

c. Choose the interval between frames. This must be matched to the phase shifter so that the chosen number of frames is taken during the time required for a 2π phase shift. Currently this is approximately one second and an inter-frame delay of 260 ms for five frames yields about the correct phase shift (90 degrees between frames is ideal but not essential). Various delays in data transfer limit the inter-frame delay to values >200 ms.

Acquire the Data

d. When done, click "OK". A new dialog box appears to allow the user to time the acquisition to the phase shift. The phase shifter is driven by a repetitive ramp with a fast return to zero phase shift. This rapidly

changing phase should not be part of the data set. The phase shifter is currently adjusted to give several full fringe shifts before resetting, so there is plenty of time to acquire the single fringe shift needed. Wait until the video image jerks marking the reset period, then click "OK".

Display the Data

e. If desired, one can now display the raw fringes. Open the "Display" menu and select "Raw Fringe Image". Pick any image and click "OK". Check the intensity by placing the cursor in the white fringes to be sure these areas are not saturated (>254). The pixel location and intensity are displayed at the upper right of the window. Pixel (1,1) is at the upper left and pixel (512,480) is at the lower right.

Make a Mask

f. Select "Folded Phase" from the "Analyze" menu. A dialog box requires you to create a mask image to proceed. Select "OK". In the new dialog box, select the option and image desired for mask creation. Usually, "Create New Blank Mask: All Good" using the first raw fringe image is a reasonable choice at this stage. You may want to edit the mask after you see the results of the unfolding process (see L, below).

Select Data Reduction Method

g. The selected image appears and you are asked to outline bad areas with the cursor. Usually, at this stage, it is advisable to simply click on "OK" and wait to correct the mask later after problems have become evident.

h. A dialog box asks which type of data reduction you desire to use. Select " Line in Fringe Image".

i. A dialog box appears asking you to choose a raw fringe image to mark a fringe. Choose any, but the first is fine.

Mark One Fringe Span

j. A raw fringe image appears. Use the cursor to drag a line between any two adjacent fringes. These should be fringes which you believe are separated by 2π phase difference. For example, the two sides of a circular fringe or two branches of a saddle fringe are not appropriate, since the phase is constant along these.

The span should be between comparable regions, for instance the center of one white fringe to the center of the next. This need not be exact, since the program will compensate for overly long or short spans, within reason (don't span two fringes, for example). Also, try to avoid regions that are messy or where the fringes are very narrow. You can re draw this span as often as you like. When satisfied, click "OK". Major problems with your choice will elicit dialog boxes with error comments.

Compute Folded Phase

k. The phase shifts between raw fringe images are computed and a dialog box appears displaying the phase shifts in radians and degrees. Click "OK" and the folded phase values are computed at each pixel. The "Fried Brain" cursor appears during long computations (there are two such long computations, each about 20 seconds long).

View Folded Phase

l. The folded phase image appears as a gray scale image with maximum phase white and minimum phase black. The range is 256 levels (0-255) with a 2π ambiguity not yet resolved. This image will closely resemble the original raw fringe pattern, but will be much more distinct. Pixel locations and intensity (phase) are displayed for the cursor location. If the image has been dimensionally calibrated, the true length of a drawn line will be displayed, otherwise, the length is given in pixels.

Compute Unfolded Phase

m. If satisfied, choose "compute unfolded phase" from the "analyze" menu.

Choose Start Point for Unfolding

n. The folded phase image reappears, asking that a starting point be selected for the unfolding process. Virtually any point will do, except bad pixels (you will be warned if you select a bad pixel). Also avoid regions with very complex structures. The best choice is a broad smoothly varying region. Note that if the fringe pattern is divided into disconnected regions with continuous regions of bad pixels, the unfolding process may or may not "bleed" through these regions depending on the quality of the raw fringe data. Click on "OK" to proceed with the unfolding.

View Unfolding Phase

o. The unfolded data appears as a gray scale image with white representing high phase (displacement) and black low. This is usually a very smooth and featureless image, with only bad (i.e. white) pixels disturbing the smooth gradations. If one sees abrupt gradient changes, or striping, it generally means that the mask must be altered to exclude bad pixels not detected by the algorithms. Often these are caused by a damaged grating which creates little discontinuous regions too small to be resolved by the video camera.

Modify Mask to Remove Problem Areas

p. To modify the mask, open the "Edit" menu and select "Mask". In the resulting dialog box, choose "Use Current Mask" and Choose the unfolded phase image for display. Other images could be used, but the

unfolded phase displays where the unfolding process is having problems.

q. Remove problem regions by drawing polygons around them. Each click anchors one vertex of the polygon at the current cursor location. When done, click the right button to draw a line from the last point to the first and fill the polygon with bad pixels. Other polygons may now be drawn until all bad regions are excluded. Errors can be fixed either by selecting "Cancel" and restarting the edit process, or by selecting "Good" and superimposing a new polygon over the region accidentally excluded previously. When done, click "OK" and return to "L" above. When asked, discard current image; this refers to the earlier unfolded phase.

Data Storage

r. All acquired images are automatically stored in a scratch file named In.img, where n is the frame number, beginning with zero. Computed images are not automatically saved to disk. It is assumed that loss of raw data caused by a power failure during a test is significantly more serious than loss of a computed data file which can be recreated in a minute or two. The scratch file is overwritten each time a new data set is acquired. To save any of the data or computed images, open the "File" menu and select either "Save" or "Save As". The latter being used if the data has been saved earlier and one wishes a new copy under a different file name. When a data set is saved as "Name", a file called Name.lst is created which stores information about the data set which is used when the set is opened again. Data sets can be reopened by using the "Open" option in the "File". MS Windows offers other options for viewing and naming files from within the File Manager.

Viewing Data

s. The data sets consist of arrays of intensity or phase values which can be displayed as gray scale or pseudo color video or monitor images.

Auxiliary Programs

We have provided two auxiliary (i.e. non-windows) programs for conversion of data sets to other formats. In general these formats are compatible with the Macintosh application "Spyglass". These conversion programs can be run under windows from the Windows Program Manager: double click on the program icon.

The two conversion programs provided are:

1. "Unf to Displacement" which opens the unfolded data file *.unf and converts it to the equivalent displacement data file using the moiré equation u=N/2f (u=displacement, N=fringe number, f=specimen grating groove density in lines per mm).

   Follow the instructions; use full path and file names for the input and output files. When prompted for the grating frequency, use the physical specimen grating frequency in lines per mm, not the "virtual" grating. In addition to converting the data, the program displays the maximum and minimum data values and the value assigned to bad pixels. These values should be noted in the data book since they will save much time when the data set is imported to Spyglass. These Max./Min. values are used to set the Color Bar (i.e. histogram) in Spyglass which adjusts the range of data displayed. This is necessary because the bad pixels are set high and distort the apparent data range.

2. "Unf to Long" the other auxiliary program takes the unfolded data file *.unf and converts it to a long integer format compatible with some display programs, including Spyglass.

Note: the data files created by both 1 and 2 above have inverted bytes compared to those expected by the Macintosh. Spyglass allows one to import such data and invert the high and low bytes to correct this problem.

APPENDIX B: FILE FORMATS USED IN FRINGE©

A. Main Program

*.IMG	Raw fringe image file. Size: 245760 byte, 512 x 480 x 8 bit binary array
*.MSK	Mask image file containing bad pixels. Size: 245760 byte, 512 x 480 x 8 bit binary array
*.DIM	Dimension image file derived from calibration process. Size: 245760 byte, 512 x 480 x 8 bit binary array
*.SHT	Shuttered image file used in one form of data reduction. Size: 245760 bytes, 512 x 480 x 8 bit binary array
*.FLD	Folded image file containing phase data with 2π ambiguity, Size: 245760 bytes, 512 x 480 x 8 bit binary array
*.UNF	Unfolded image file containing phase data with 2π ambiguity removed. Size: 491520 bytes, 512 x 480 binary word array: high byte contains integer phase value (fringe number) low byte contains fractional phase value (0 to 2Π).

B. Auxiliary Programs

*.DSP	Displacement file containing data derived from *.unf using the moiré equation u=n/2f (run auxiliary program " Unf to Displacement"). Size: 983040 bytes, 512 x 480 x 16 bit floating point binary double word array.
*.LNG	Unfolded image file in long integer format derived from *.Unf (run auxiliary program "Unf to Long"). Size: 983040 bytes, 512 x 480 binary double word array.

NOTE 1: *.DSP and *.LNG have an MS DOS byte structure which is inverted relative to that of the Macintosh. Spyglass offers the option to invert high and low bytes and this should be used for these two file types.

NOTE 2: The image data are in raster format with pixel (1,1) at the upper left and (512,488) at the lower right. The data are arranged so that the pixels are stored row by row starting with the top row reading left to right. A complication comes in that MS Windows orients pixels starting at the lower left ((0,0) in the usual coordinate arrangement). A significant amount of computation time is involved in reordering of pixels for display. This is necessary to avoid inverted images relative to the video monitor.

Dimensioning of the data to mirror specimen dimensions is also complicated by these effects, as well as by differences in aspect ratios among the video camera, digitizer, MS Windows and the display monitor(s). It is best to include some sort of fiducial marks on the specimen itself. We often include small scratches in the specimen grating at known locations to provide horizontal and vertical dimension data.

The INEL FRINGE© program provides an internal dimension capability in one dimension (applied to pixels in both dimensions). However, this is intended only as a visual aid and should not be used as a permanent solution to the dimensioning problem.

NOTE 3: One is still faced with more subtle distortions and dimension errors caused by the camera lens, CCD chip irregularities and errors in clock rate (pixel transfer rate) at the camera or digitizer. Less important distortion errors occur because of poorly designed or adjusted monitors. These don't affect the actual data, but can be confusing to the viewer. Circles may appears as ellipses, or outer edges of the images may be missing.

Finally, errors due to non-linearity in the gain circuits of the camera or digitizer can cause problems with the data. It is also possible for there to be a pixel to pixel variation in gain due to manufacturing variations in the chip. Some pixels may actually be bad. One pays a high premium for perfect chips.

Unless one pays very careful attention to all of these factors, one can not expect to fully exploit the resolution available with phase shifting methods. Instead, we have taken the approach that the phase shifting lifts the considerable burden of manual data reduction from the shoulders of the researcher. Even if one only duplicates the resolution achievable by manual reduction, one is well ahead of the game. In reality I believe that one can easily achieve an order of magnitude improvement in displacement resolution using standard components as was done in the INEL interferometer.

APPENDIX C: EVALUATIONS

In an attempt to evaluate the accuracy of the phase evaluating algorithms, we created a set of synthetic fringes derived from a known (noise free) phase map . this resulted in 5 fringe images with a known but unequal relative phase shift between successive images (0, 30, 90, 180, 300 degrees).

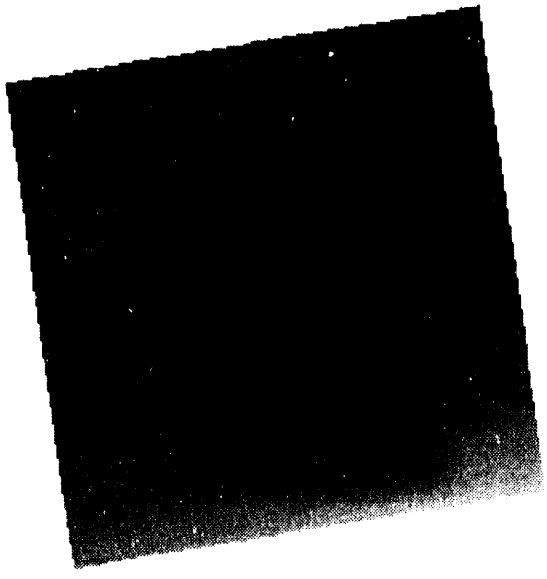

Figure 1. Original Synthetic Phase Map

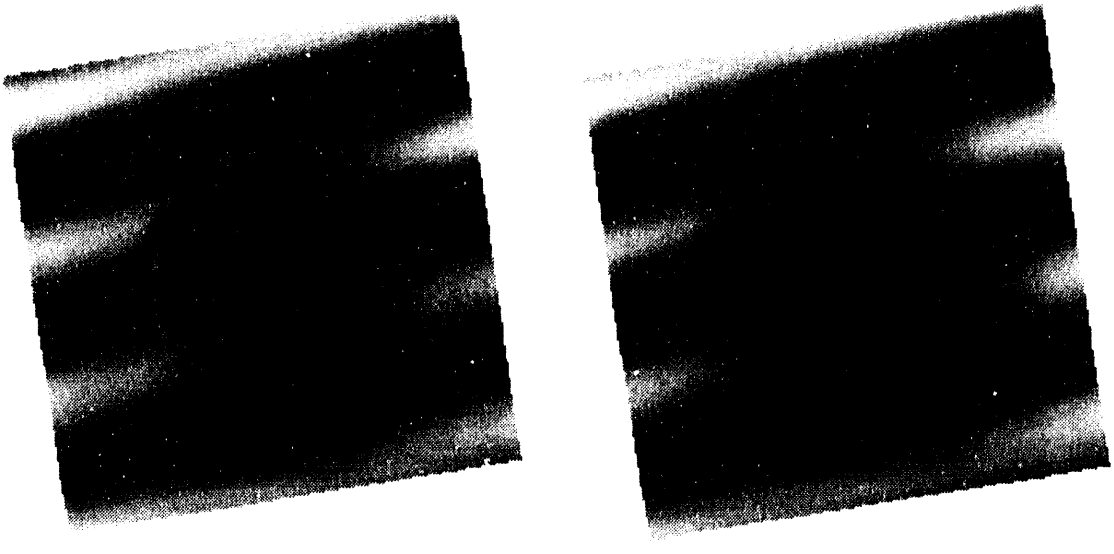

First of 5 Phase Shifted Fringe Images Next of 5 Phase Shifted Fringe Images

Figure 2. Additionally, two shuttered images were synthetically generated. These represented fairly poor data in that the "beam intensities" represented by these images were quite different in average intensity (with intensity ratios as

poor as 16 to 1 at some pixels), had Gaussian like intensity variation superimposed on the fringe variations, and these Gaussians were not centered on the same spot. An additional complication was that the Gaussians were inverted. On the plus side, the data are noise free (i.e. each pixel is accurate within truncation errors and not speckle or diffraction noise or optical aberrations exist).

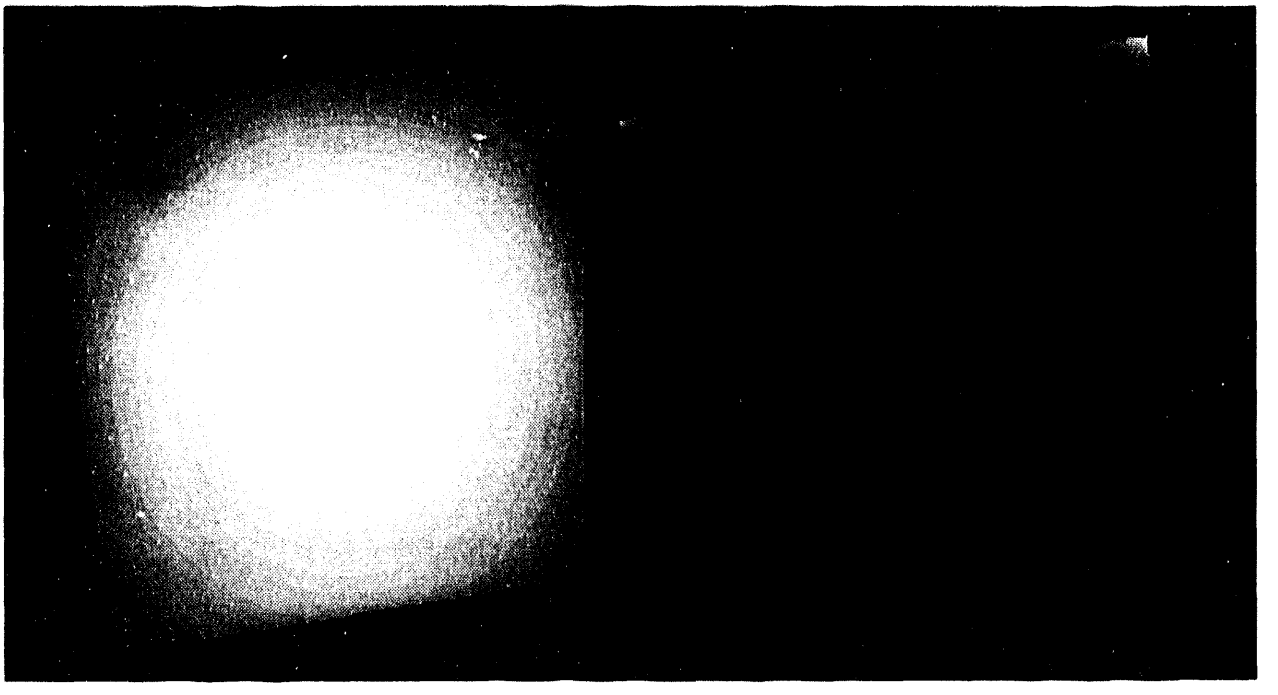

Left Hand Beam Image Right Hand Beam Image

Figure 3. Shuttered Beam Images

These fringe and shuttered beam images were analyzed using both the shuttered and the fringe span techniques described earlier. The calculated phase was then subtracted from the original phase on a pixel by pixel basis. These differences were used to compute statistics to compare the methods. Table 1 shows the phase and error data for the four different phase calculations (the line pick method was done three times with different lines picked).

Note: the phases are in degrees and errors are in fringes or waves (1 fringe = 360 degrees). The average and standard deviations of errors are computed over all valid pixels. The standard deviation is the best descriptor of the relative and absolute errors of the computations. In contrast, for perfect data and perfect phase calculations, the error due to truncations in integer format would be expected to result in an RMS phase error of 0.0011 waves (fringes), or 0.396 degrees. Naturally, noisy data may significantly worsen the actual variations in the data.

TABLE 1: COMPUTED PHASE ERRORS

ERROR: TEST A: SHUTTERED	ERROR: TEST B: LINE PICK 1	ERROR: TEST C: LINE PICK 2	ERROR: TEST D: LINE PICK 3	DATA TYPE
not available	30.19	30.20	32.08	PHASE SHIFT 2
"	93.40	92.12	97.30	P.S. 3
"	181.06	181.22	189.10	P.S. 4
"	299.17	302.79	302.07	P.S. 5
0.0017	0.0018	0.0027	0.0015	COMPUTED PHASE ERROR STD. DEVIATION
-.0028	-.0063	-.0080	-.0169	AVG. PHASE ERROR
-.0088	-.0127	-.0158	-.0222	MIN. PHASE ERROR
0.0028	-.0012	-.0016	-.0107	MAX. PHASE ERROR

APPENDIX D: PUBLICATIONS OF INTEREST

1. A. Livnat and D. Post, "The governing equations for moiré' interferometry and their identity to equations of geometrical moiré," *Experimental Mechanics,*, pp. 360-366, Dec., 1985.
2. F.L. Dai, J. McKelvie and D. Post, "An interpretation of moiré interferometry from wavefront interference theory," *Optics and Lasers in Engineering*, v. 12, n. 2, pp. 101-108, 1990.
3. T.W. Shield and K.S. Kim, "Diffraction theory of optical interference moiré and a device for production of variable virtual reference gratings: a moiré microscope," , v. 31, n. 2, pp. 126-134, June 1991.
4. D. Post, "Moiré interferometry for Composites," Manual on Experimental Methods for Mechanical Testing of Composites, R.L. Pendleton and M.E. Tuttle, editors, Society for Experimental Mechanics, Bethel, Connecticut, pp. 67-80.
5. D. Joh, "Optical precision alignment of diffraction grating mold in moiré interferometry," *Experimental Techniques*, , pp. 19-22, May/June, 1992.
6. J. Guild, "*The Interference Systems of Crossed Diffraction Gratings*," Clarendon Press, Oxford, 1956.
7. F.M. Gerasimov, Applied. Opt., Vol. 6, p. 1861, 1967.
8. D. Post, "Analysis of moiré fringe multiplication phenomena," *Applied. Optics*, Vol. 6, p. 1938-1942, Nov. 1967
9. D. Post, "Moiré fringe multiplication with a non symmetrical doubly blazed reference grating," *Appiied. Optics*, Vol. 10, pp. 901-907, April, 1971.
10. R.E. Rowlands and J.H. Vallem, "On replication for moiré fringe multiplication," *Experimental Mechanics*, Vol. 20, No. 5, pp. 167-169, May 1980.
11. C.A. Walker, J. McKelvie, "A practical multiplied moiré system," *Experimental Mechanics*, Vol. 18, no. 8, pp. 316-320, Aug. 1978.
12. D. Post and Baracat, "High sensitivity moiré interferometry-a simplified approach," *Experimental Mechanics*, Vol. 21, No. 3, pp. 100-104, March, 1981.
13. D. Post, "Optical Interference for Deformation Measurements--Classical, Holographic and Moiré Interferometry," *Mechanics of Nondestructive Testing*, p. 1-53, W.W. Stinchcomb, Ed., Plenum Press, NY, 1980.
14. B. Han, D. Post, "Immersion interferometer for microscopic moiré interferometry," *Experimental Mechanics*, Vol. 32, No. 1, pp. 38-41, March, 1992.
15. V.A. Deason and M.B. Ward, "A compact portable diffraction moiré interferometer," *Proceedings of the 3rd International Conf. on Laser Interferometry*, SPIE Vol. 1162, pp. 26-35, 7-9 Aug., 1989.

16. J. McKelvie, C.A. Walker, P.M. MacKenzie, "A workaday moiré interferometer: conceptual and design considerations; *etc.*" *Proceedings of the Conference on Photomechanics and Speckle Metrology*, SPIE Vol. 814, pp. 464-474, 1987.

17. V.A. Deason, M.B. Ward, "Phase shifting hand-held diffraction moiré interferometer," *Proceedings of the SPIE Second International Conf. on Photomechanics and Speckle Metrology*, Vol. 1554B, pp. 390-398, July 22-26, 1991

18. V.A. Deason, "High pulse rate interferometry using a ruby laser and a Cordin model 330A camera," *Optics and Lasers in Engineering*, v. 19, nos. 1-3, pp 161-170, (1993).

19. K. Arakawa, R.H. Drinnon, Jr., M. Kosai, and A.S. Kobayashi, "Dynamic fracture analysis by moiré interferometry," *Experimental Mechanics*, pp. 306-309, Dec. 1991.

20. J.M. Huntley and J.E. Field, "High resolution moiré photography: application to dynamic stress analysis," *Optical Engineering*, Vol. 28, No. 8, pp. 926-933, Aug. 1989.

21. F.X. Wang, P. Ifju and B.S.J. Kang, "High temperature moiré interferometry using zero thickness grating," *Proceedings of the SEM VII International Congress on Experimental Mechanics,*, vol. 1, pp. 727-731 , June 8-11, 1992.

22. D. Post, *Handbook on Experimental Mechanics*, Ch. 7, Ed. A.S. Kobayashi, Prentis Hall, Englewood Cliffs, NJ, 1987.

23. V.A. Deason, M.B. Ward, "A convenient system for the manufacture of holographic diffraction gratings," *Proceedings of the Third International Conference on Laser Interferometry*, SPIE Vol. 1162, pp. 54-61, 7-9 Aug., 1989.

24. V.A. Deason, Gordon Lassahn, "Novel approaches to automated reduction of phase-shifted interferograms," *Proceedings of the* 4th *International Conference on Laser Interferometry*, SPIE Vol. 1553, pp. 569-582, 22-24 July, 1991.

25. J.H. Bruning, D.R. Herriott, J.E. Gallagher, D.P. Rosenfeld, A.D. White, and D.J. Brangaccio, Digital wave front measuring interferometer for testing optical surfaces and lenses," *Applied. Optics*, Vol. 14, p. 2693, 1974.

26. L. Salbut, K. Patorski and M. Kujawinska, "Polarization approach to high sensitivity moiré interferometry," *Optical Engineering*, Vol. 31, No. 3, pp. 434-439, Mar. 1992.

27. S.M. Graham and R.J. Sanford, "The influence of grating characteristics on moiré fringe multiplication," *Experimental Mechanics*, pp. 329-335, Dec. 1988.

28. D. Post, B. Han and P. Ifju, "*High Sensitivity Moiré: Experimental Analysis for Mechanics and Materials*," Springer Verlag, 1993.

29. V.A. Deason, "An overview of diffraction moire methods and systems," SPIE Critical Review of Technology, Vol. CR 46, pp 60 - 87, Nov. 1992.

30. J.S. Epstein, "Applications of moire interferometry to mechanical behavior of materials, "SPIE Critical Review of Technology, Vol. CR 46, pp 88 - 126, Nov. 1992.

31. G.D. Lassahn, J.K. Lassahn, P.L. Taylor, V.A. Deason, "Multiphase fringe analysis with unknown phase shifts," to be published in *Optical Engineering*.

32. Interferogram Analysis, D. W. Robinson, G.T Reid, eds. Institute of Physics Publishing, Bristol and Philadelphia, 1993, ISBN 0-7503-0197-X.

APPENDIX E: MORE DETAILED DESCRIPTION OF DATA ANALYSIS PROCESS (TO BE PUBLISHED IN *OPTICAL ENGINEERING*)

Multiphase Fringe Analysis With Unknown Phase Shifts

AUTHORS: Gordon D. Lassahn, Paul L. Taylor, Vance A. Deason: INEL, EG&G Idaho, Inc. Jeffrey K. Lassahn: University of Oregon

ABSTRACT

We present methods for determining the phase shifts in multiphase fringe analysis from the fringe image data itself, thus eliminating the requirement for prior knowledge or accurate control of the phase shifts. We also discuss methods for calculating the folded (wrapped) and unfolded phases, and quote the accuracy of the fringe analysis method for an example in which the correct result is known.

Introduction

Fringe analysis is a measurement tool in which images of optical interference fringes are used to indicate spatial variations of some physical parameter such as displacement or gas density. In a typical application of diffraction Moire fringe analysis, for example, two coherent light beams illuminate a diffraction grating and two diffracted beams interfere with each other to produce a fringe pattern, the details of which depend on distortions either of the grating or of the wavefronts of the incident light beams. In multiphase fringe analysis measurements, several images of interference fringes are recorded from the same experiment, with each successive image having a different amount of phase shift added to one of the incident light beams. The advantages of having multiple, phase-shifted interference fringe images are two: resolution of certain ambiguities in data interpretation, and less sensitivity to noise in the data.

The older methods of interpreting multiphase fringe data require that the phase shifts for the several fringe images are known or are unknown but all the same. However, multiphase fringe analysis can be done with phase shifts of arbitrary values (except for certain degenerate combinations of values)[1]. It is generally conceded that, even though the phase shift values can be arbitrary, they must be known accurately. This means that the phase shift values must be set accurately to some pre-selected values, which requires sophisticated phase-shifting hardware; or, that simpler phase-shifting hardware can be used if there is some method for accurately measuring the phase shifts. Lai and Yatagai[2] report a method of recording extra fringe data that allows easy determination of the phase shifts. Okada, Sato, and Tsujiuchi[3] report an iterative method for extracting the phase shift values from the fringe image data, assuming that there is available some reasonable first guess at the phase shift values. The results they discuss use a large number (32) of phase-shifted fringe images and random errors in the first guess phase shift values; there is some question about whether their method can work with a small number (3 to 5) of fringe images or with first guess values that are not random (all too large, for example). Farrell and Player[4] report a method of extracting the phase shift values from the fringe images using a Lissajous figure calculation, which appears to be satisfactory.

This report discusses two alternate methods for eliminating this requirement for uniform or known phase shifts in the analysis of multiphase interference fringe data. One method requires the recording of two extra images along with the fringe image data, and the other requires no extra data but does require a little operator interaction.

Statement of the Problem

We are given a set of K images of fringe patterns, each produced by the interference of two coherent light beams. The phase difference between the two light beams is different for the K different images; let Δ_k be the phase shift added to one of the incident light beams when recording image k, k=2,3...K, relative to the phase for image 1. Then the intensity at the pixel at column i and row j in image k can be written as

$$I_k(i,j) = A(i,j) + B(i,j)\cos(\Phi(i,j)+\Delta_k) + \text{error}, \qquad (1)$$

where $\Phi(i,j)$ is the phase difference between the two beams at pixel i,j for image 1. This Φ is the quantity we wish to determine. The intensities I are measured in the experiment; they are simply the brightnesses of the pixels in the given images of the fringe patterns. A(i,j) and B(i,j) describe the intensities of the two incident beams and the fringe contrast; A and B are assumed to be smooth, slowly varying functions of i and j. The error is assumed random and unknown and small.

Calculation of the Folded Phase

For any pixel, we can express the phase Φ as

$$\Phi(i,j) = \Psi(i,j) + 2\Pi N(i,j) \qquad (2)$$

where N is some integer and $0 \leq \Psi < 2\Pi$. This Ψ is called the folded or wrapped phase. We can calculate Ψ if we know Δ_k and assume that A and B are independent of k, for any given i,j. For each pixel, we rewrite Equation 1 (not bothering to write the row and column indexes i and j) as

$$I_k = P1 + P2\cos(\Delta_k) - P3\sin(\Delta_k) + \text{error}, \qquad (3)$$

where $P1 = A$, $P2 = B\cos(\Psi)$, and $P3 = B\sin(\Psi)$. This represents K equations in the 3 unknowns P1, P2, and P3. If K is greater than 3, we can calculate the 3 unknowns using a linear least squares calculation. (This approach has been used by others[1].) The coefficient matrix for the least squares calculation is the same for all pixels; therefore, we can solve the set of least squares equations once and for all, rather than solving separately for each pixel. Then P2 and P3 can be found for each pixel by calculating a few simple sums, and then the phase at that pixel can be calculated by

$$\Psi = \text{atan2}(P3,P2) \qquad (4)$$

where "atan2" is a function that calculates an angle when it is given the opposite side and the adjacent side of a right triangle. We also calculate

$$B = \text{sqrt}(P3*P3 + P2*P2) \qquad (5)$$

as an indicator of the validity of the phase calculation for this pixel. If B is too small, either the fringes are of very low contrast or something else has gone wrong with the phase calculation. In this case, the pixel is declared invalid and no phase is calculated for that pixel. Note that we do not need to calculate the value of P1, although we must allow it to be an adjustable parameter in order to achieve a meaningful fit of Equation 3 to the data.

Unfolding the Phase

Unfolding or unwrapping the phase is done by a procedure that is in most ways quite standard, adding multiples of 2Π to the folded phase at each pixel to make that pixel's unfolded phase close to that of its neighboring pixels. The present procedure uses an adaptive criterion to decide whether each pixel fits with its neighbors well enough to allow unfolding. If none of the still-folded pixels fits well enough to be unfolded, the criterion is relaxed to some maximally tolerant value. When some pixels can be unfolded, the criterion is gradually made more stringent. This has the effect of unfolding the best fitting pixels first and delaying the questionable pixels, which tends to avoid making unfolding errors early in the process and allowing those errors to affect later unfolding.

Calculating Phase Shifts between Fringe Images

The procedure described earlier for calculating the folded phase Ψ requires knowledge of Δ_k, the phase difference between the two light beams for fringe pattern k relative to that for fringe pattern 1. We describe two alternate methods for determining Δ_k, referred to as the line-drawing method and the beam-shuttering method.

Line-Drawing Method

To estimate the Δ_k values, we first specify a straight line segment on the images, such that the line spans approximately one full fringe cycle in a region where the phase Φ is approximately a linear function of position, where the fringe that is spanned is fairly broad, and where there is not too much noise in the raw data. In simple terms, the intensity versus position along this line is fitted with a cosine function to determine a phase Δ_k for each of the fringe images. This process is explained in more detail as follows:

> Let s be the position along this line, and let Φ along this line be specified by a polynomial approximation:

$$\Phi = \Phi(s=0) + \Phi(s) \quad (6)$$

where $\Phi(s=0)$ is simply the phase Φ at one end of the line and

$$\Phi(s) = \alpha_1 s + \alpha_2 s^2 \ldots + \alpha_m s^m \ldots + \alpha_M s^M, \; m=1,2,\ldots M. \quad (7)$$

The number of terms M is specified beforehand to be some low value, like 2. Allowing M to be greater than 1 accounts for nonlinearity in the phase versus position relationship. The α_m are to be determined. As a first estimate, α_1 is simply 2Π divided by the line length, and the other α_m are zero. (These α values would be exactly correct for the ideal situation of linear phase versus position with no noise.) For fringe image k, the intensity along the selected line can be written as

$$I_k(s) = A + B\cos(\Phi(s)+\Delta_k) = A + B\cos(\Phi(s)+\Lambda_k) \quad (8)$$

where $\Lambda_k = \Delta_k + \Phi(s=0)$. We assume that the number of pixels along the specified line segment is greater than K+M. Then we can determine the Λ_k and the α_m by a non-linear least squares fitting procedure. This requires first estimates for the α_m, which we already have, and for the Λ_k, which are obtained as follows:

$$E = \int I_k \cos(\Phi(s))\, \alpha_1\, ds = \int I_k \cos(\Phi)\, d\Phi = B\cos(\Lambda_k)\,/\,2 \quad (9)$$

and

$$F = \int I_k \sin(\Phi(s))\, \alpha_1\, ds = \int I_k \sin(\Phi)\, d\Phi = -B\sin(\Lambda_k)\,/2 \quad (10)$$

assuming that $\Phi(s)=\alpha_1 s$ and the line segment is one cycle long. The integrals F and E can of course be approximated by sums over the pixels in the line segment, which then allows the first estimate

$$\Lambda_k = -\,\mathrm{atan2}(F,E). \quad (11)$$

After these first estimates are obtained, better values for the Λ_k and the α_m can be obtained by the usual iterative, non-linear least squares fitting procedure. Finally, we can do the trivial (and not really necessary) transformation

$$\Delta_k = \Lambda_k - \Lambda_1. \quad (12)$$

This is the desired result.

Beam-Shuttering Method

There is a second method for calculating the Δ_k, which does not require any operator intervention (drawing a line spanning one fringe). However, it does require that we record two additional images, one with the first incident beam blocked and the other with the second incident beam blocked. Thus, these two images represent simply the intensities of the two separate incident beams. These two additional images allow us to, in effect, eliminate the unknowns A and B from Equation 1. We must still cope with the ambiguity in the inverse cosine function; this is done by sampling the images at a number of different pixels and looking for consistent choices about which branch of the inverse cosine function to use. Taking samples at several pixels also tends to average out whatever noise may be present. Details of this process are as follows:

For convenience, we will refer to these two shuttered-beam images as L and R. For any pixel, we can use the L and R image intensity values to calculate a "normalized intensity" for that pixel in the k-th fringe image:

$$J_k = (I_k - L - R)/(2[LR]^{1/2}). \quad (13)$$

Except for the effects of noise or measurement error, this normalized intensity is equal to the cosine of the total phase for that pixel in fringe image k:

$$\cos(\Phi + \Delta_k) = J_k. \quad (14)$$

In this system, we assume that the phase shift between two successive fringe images is never greater than Π. With this restriction in mind, to calculate the phase difference between two successive fringe images _ say $\Delta_2 - \Delta_1$, for example _ we look at the same pixel in the two normalized fringe images. If either of these two normalized intensities has an absolute value close to 1.0 (say, greater than 0.9), we do not use this pixel to estimate the phase difference, because such values give excessive sensitivity to small errors in the data. If the absolute values of the normalized intensities are acceptably far from 1.0, then the absolute value of the phase difference is given by one of two calculations:

$$D_1 = \mathrm{ABS}[\arccos(J_2) - \arccos(J_1)] \quad (15)$$

and either of

$$D_2 = ABS[\arccos(J_2) + \arccos(J_1)] \quad (16)$$

or

$$D_2 = 2\Pi - ABS[\arccos(J_2) + \arccos(J_1)] \quad (17)$$

depending on which D_2 value is less than Π. There is no way to tell from this pixel alone which of D_1 or D_2 is the correct phase difference. We enter both of these values in a list of pairs of possible values for Δ_2-Δ_1. We also make a rough estimate of the uncertainty of these two values, based on the assumption of equal uncertainties for all normalized intensity values, and enter that uncertainty value into a list. We then repeat this process for perhaps a hundred or a few hundred other pixels, thus generating a list of pairs of values with perhaps a hundred entries and a list of uncertainty values.

After the list is made, we compare each entry in the list with every other entry in the list of pairs of Δ_2-Δ_1 values. Ideally, each entry should contain one correct value and one incorrect value, so one value from one entry should be equal to one value from the other entry and the other two values should be different (although perhaps not much different). Therefore, in the comparison, if we find two approximately equal values (within 0.1 radian) and two other values that are significantly different (by more than 0.2 radian), we consider the two nearly equal values to be reasonable estimates of the correct Δ_2-Δ_1 value and we include these two values in a weighted average that will give a (hopefully) good estimate of the correct value. The weighting coefficient for each value included in the average is the inverse of the square of the uncertainty of that value.

Accuracy

To check these procedures, we synthesized a set of 5 fringe images and 2 shuttered images. The incident beam phase differences Δ_k for the 5 fringe images are 0 (by definition for the first fringe image), 30, 90, 180, and 300 degrees. This synthetic data set includes no noise except for the truncation error associated with representing the intensities with 8-bit integers. Both the average intensity and the contrast are slowly varying functions of position. Figure 1 shows the phase, represented as brightness in this figure. The total range of the phase values is about 4 fringes. The first fringe image is shown in Figure 2. This data set includes local extrema (closed loop fringes) and a saddle point in the phase map, which present no special difficulty to the algorithms presented here.

We list here the results of one analysis using the shuttered images, which should be the same for repeated analyses of the same data set, and three analyses using the line-drawing method without the shuttered images, which may give different (hopefully not much different) results depending on where the operator draws

the line. The results of these four analyses are listed in Table 1. The column headed "S.B." gives the results for the first analysis which uses the shuttered images, and the next three columns headed "L.D.1", "L.D.2", and "L.D.3" give the results for the three analyses using the line-drawing method. The column headed "IDEAL" gives the correct or ideal values.

Table 1 lists the calculated phase shifts Δ_k for the 4 analyses, in degrees. The first analysis, which used the shuttered images, is a little more accurate in this respect than the other three which used the line-drawing method.

Table 1 also lists five indicators of the error in the calculated phase for each of the four analyses, obtained by direct comparison of the fringe analysis program's output with the known correct phases for this synthetic data set. In this comparison, any overall difference that is a multiple of 2Π is ignored. Perhaps the most useful error indicator is the standard deviation of the distribution of the errors in the calculated phase. In these calculations, the results of the phase analysis program were output in the form of integer values with a truncation error of $\pm 1/512$ fringe, so the minimum expected standard deviation is 0.0011 fringe even if there are no calculation errors and no noise in the input data. The average error is usually not significant in practical applications. The minimum and maximum error values are of course affected by the average error value; the error range, the difference between the maximum error and the minimum error, is usually a more meaningful error indicator than the minimum or maximum values themselves.

It is interesting to note that errors of several degrees in the phase shift values do not seem to cause a significant increase in the errors in the final calculated phases at the individual pixels. In the worst case in Table 1, the error standard deviation is only 0.0027 fringe and the error range is only 0.0142 fringe.

The tests represented in Table 1 are for data with no noise (except for roundoff error). To evaluate these fringe analysis procedures with more realistic data, we added noise to the fringe images used in the previous tests. The noise was approximately Gaussian distributed, with root-mean-square magnitudes (standard deviations) of 2, 5, 10, and 20 intensity units. The full range of intensity values in the fringe images is 0 through 255, and the average intensity and the fringe amplitude (A and B in Equation 1) are 100 and 50 at the center of the fringe pattern (they vary a little with position). In some cases, particularly with the larger noise levels, the added noise caused the intensities of some pixels to extend beyond the acceptable range of 0 to 255; in these cases, the out-of-range intensity value was simply truncated to force it to be within range.

The noisy data sets were analyzed in the same way as the no-noise data, with one analysis (S.B.) using the shuttered images and three analyses (L.D.1, L.D.2, and L.D.3) using the line-drawing method without the shuttered images. The results

are listed in Tables 2 through 5. In these tables, the STANDARD DEVIATION value in the IDEAL column is a theoretical estimate of the root-mean-square error in the individual pixel phase values, due to the noise in the fringe images, assuming no error in the overall phase shifts Δ_k. With the larger noise levels, a significant fraction of the pixels were declared "BAD" by the fringe analysis program. They could not be analyzed because the fringe contrast appeared too low or because the noisy intensity values were in some way not compatible with the expected form. Tables 4 and 5 indicate the percentage of pixels declared bad for noise levels of 10 and 20. For lower noise levels, the percentage of bad pixels was less than 0.01 %.

Tables 2-5 indicate that the calculation of phase shifts using the shuttered images is much more susceptible to noise than is the line-drawing method which shows surprisingly little sensitivity to the noise levels tested here. As with the no-noise test, we see that relatively large errors in the calculation of the phase shift values do not seem to significantly increase the noise in the final result, the phases calculated for the individual pixels. That is, for each of the tables, the first column compared to the next three columns indicates relatively large errors for the overall phase shifts (PHASE SHIFT Δ_k) but comparable root-mean-square errors for the individual pixel phases (STANDARD DEVIATION). This conclusion is further supported by the observation that the actual STANDARD DEVIATION values, including the effects of the errors in the overall phase shifts Δ_k, are not much larger than the IDEAL STANDARD DEVIATION values predicted with the assumption of no errors in the overall phase shifts Δ_k. For example, in Table 5, the Δ_k values in the first column have errors as large as 21, 25, and 23 degrees, which seem quite large; but, the root-mean-square error in the individual pixel phases (STANDARD DEVIATION) for this case is 0.0441 fringes, comparable with the STANDARD DEVIATION values in the L.D. columns which have smaller Δ_k errors and only slightly larger than the estimated ideal STANDARD DEVIATION value of 0.0429 fringes.

Conclusions

Phase-shifted fringe analysis can be a highly automated process with small errors in the final results. The system used here requires, as a minimum, that the operator choose a starting point for the unfolding process; in a more interactive option, the operator must also mark a line spanning one fringe in a low-noise region of the image. With synthetic fringe image data, this system gives phase calculation errors with a standard deviation no worse than 0.0027 for input data with no noise, and it gives approximately the theoretically predicted phase errors for noisy data. This analysis can be done without any stringent requirement for phase shift values, such as particular values, regularly-spaced values, or accurately controlled values.

Acknowledgment

This work was supported by the U. S. Department of Energy under DOE Field Office, Idaho, Contract No. DE-AC07-76ID01570.

References

1. J. E. Greivenkamp, "Generalized data reduction for heterodyne interferometry", *Optical Engineering* **23**(4), 350-352 (1984).

2. Guanming Lai and Toyohiko Yatagai, "Generalized phase-shifting interferometry", *Journal of the Optical Society of America A* **8**(5), 822-827 (1991).

3. Katsuyuki Okada, Atsushi Sato, and Jumpei Tsujiuchi, "Simultaneous calculation of phase distribution and scanning phase shift in phase shifting interferometry", *Optics Communications* **84**(3&4), 118-124 (1991).

4. C. T. Farrell and M. A. Player, "Phase step measurement and variable step algorithms in phase-shifting interferometry", *Measurement Science and Technology* **3**, 953-958 (1992).

CAPTIONS:

Table 1 Fringe Analysis Results with No Noise.

Table 2 Fringe Analysis Results with Noise = 2.

Table 3 Fringe Analysis Results with Noise = 5.

Table 4 Fringe Analysis Results with Noise = 10.

Table 5 Fringe Analysis Results with Noise = 20.

Fig. 1 Phase map for synthetic data set. Phase is represented as brightness in this figure. The total phase range is about 4 fringes (8_ radians).

Fig. 2 The first fringe image of the synthetic data set.

Table 1: Fringe Analysis Results with No Noise

S.B.	L.D.1	L.D.2	L.D.3	IDEAL	
29.97	30.19	30.20	32.08	30.00	PHASE SHIFT $_2$ [degrees]
90.19	93.40	92.12	97.30	90.00	PHASE SHIFT $_3$ [degrees]
179.21	181.06	181.22	189.10	180.00	PHASE SHIFT $_4$ [degrees]
299.04	299.17	302.79	302.07	300.00	PHASE SHIFT $_5$ [degrees]
0.596	0.647	0.976	0.556	0.406	STAND. DEV. [degrees]
0.0017	0.0018	0.0027	0.0015	0.0011	STAND. DEV. [fringes]
-1.018	-2.263	-2.880	-6.101	0.0000	AVERAGE ERROR [degrees]
-.0028	-.0063	-.0080	-.0169	0.0000	AVERAGE ERROR [fringes]
-3.162	-4.588	-5.693	-8.007	-0.703	MINIMUM ERROR [degrees]
-.0088	-.0127	-.0158	-.0222	-.0020	MINIMUM ERROR [fringes]
0.993	-0.445	-0.560	-3.864	0.703	MAX. ERROR [degrees]
0.0028	-.0012	-.0016	-.0107	0.0020	MAX. ERROR [fringes]
4.155	4.143	5.133	4.143	1.406	ERROR RANGE [degrees]
0.0116	0.0115	0.0142	0.0115	0.0039	ERROR RANGE [fringes]

Table 2: Fringe Analysis Results with Noise = 2

S.B.	L.D.1	L.D.2	L.D.3	IDEAL	
34.77	32.07	28.75	31.93	30.00	PHASE SHIFT $_2$ [degrees]
101.67	93.68	88.89	92.97	90.00	PHASE SHIFT $_3$ [degrees]
192.19	183.88	179.88	179.07	180.00	PHASE SHIFT $_4$ [degrees]
300.33	296.85	301.29	293.33	300.00	PHASE SHIFT $_5$ [degrees]
3.796	3.823	3.828	3.843	1.593	STAND. DEV. [degrees]
0.0105	0.0106	0.0106	0.0107	0.0044	STAND. DEV. [fringes]
-10.75	-5.634	-4.129	-3.429	0.0000	AVERAGE ERROR [degrees]
-.0299	-.0157	-.0115	-.0095	0.0000	AVERAGE ERROR [fringes]

Table 3: Fringe Analysis Results with Noise = 5

S.B.	L.D.1	L.D.2	L.D.3	IDEAL	
37.97	29.16	27.79	30.54	30.00	PHASE SHIFT $_2$ [degrees]
111.85	86.00	89.24	90.02	90.00	PHASE SHIFT $_3$ [degrees]
199.56	178.88	187.37	181.34	180.00	PHASE SHIFT $_4$ [degrees]
302.87	299.85	305.21	303.72	300.00	PHASE SHIFT $_5$ [degrees]
5.358	5.357	5.388	5.345	3.878	STAND. DEV. [degrees]
0.0149	0.0149	0.0150	0.0148	0.0108	STAND. DEV. [fringes]
-15.99	-2.930	-6.778	-5.590	0.0000	AVERAGE ERROR [degrees]
-.0444	-.0081	-.0188	-.0155	0.0000	AVERAGE ERROR [fringes]

Table 4: Fringe Analysis Results with Noise = 10

S.B.	L.D.1	L.D.2	L.D.3	IDEAL	
40.13	35.34	28.94	29.96	30.00	PHASE SHIFT $_2$ [degrees]
108.81	96.68	84.31	85.52	90.00	PHASE SHIFT $_3$ [degrees]
199.01	180.21	181.52	178.64	180.00	PHASE SHIFT $_4$ [degrees]
296.49	295.09	306.12	298.23	300.00	PHASE SHIFT $_5$ [degrees]
8.950	8.851	8.934	8.865	7.715	STAND. DEV. [degrees]
0.0249	0.0246	0.0248	0.0246	0.0214	STAND. DEV. [fringes]
-13.90	-5.534	-4.618	-2.525	0.0000	AVERAGE ERROR [degrees]
-.0386	-.0154	-.0128	-.0070	0.0000	AVERAGE ERROR [fringes]
0.48	0.49	0.54	0.52	0.00	% BAD PIXELS

Table 5: Fringe Analysis Results with Noise = 20

S.B.	L.D.1	L.D.2	L.D.3	IDEAL	
51.31	33.74	27.23	30.36	30.00	PHASE SHIFT $_2$ [degrees]
115.27	87.51	91.53	90.93	90.00	PHASE SHIFT $_3$ [degrees]
203.44	181.52	171.45	181.37	180.00	PHASE SHIFT $_4$ [degrees]
299.42	305.78	295.42	295.90	300.00	PHASE SHIFT $_5$ [degrees]
15.87	15.85	15.92	15.77	15.43	STAND. DEV. [degrees]
0.0441	0.0440	0.0442	0.0438	0.0429	STAND. DEV. [fringes]
-18.97	-6.050	-1.101	-3.891	0.0000	AVERAGE ERROR [degrees]
-.0527	-.0168	-.0031	-.0108	0.0000	AVERAGE ERROR [fringes]
19.63	18.87	19.03	18.76	0.00	% BAD PIXELS

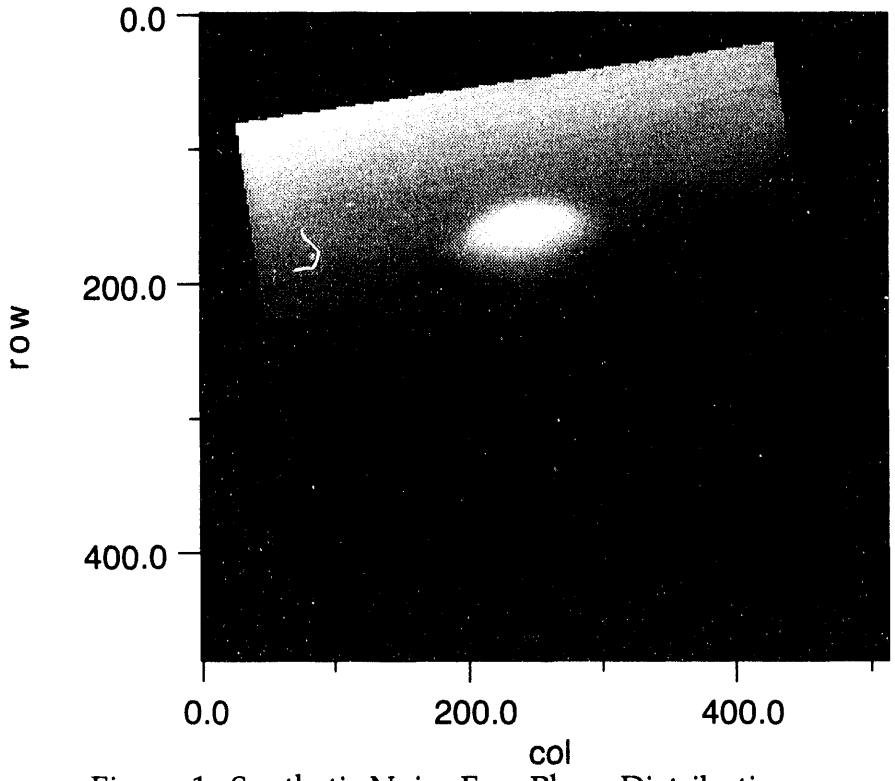

Figure 1: Synthetic Noise Free Phase Distribution Used to Generate Noisy Fringe Data

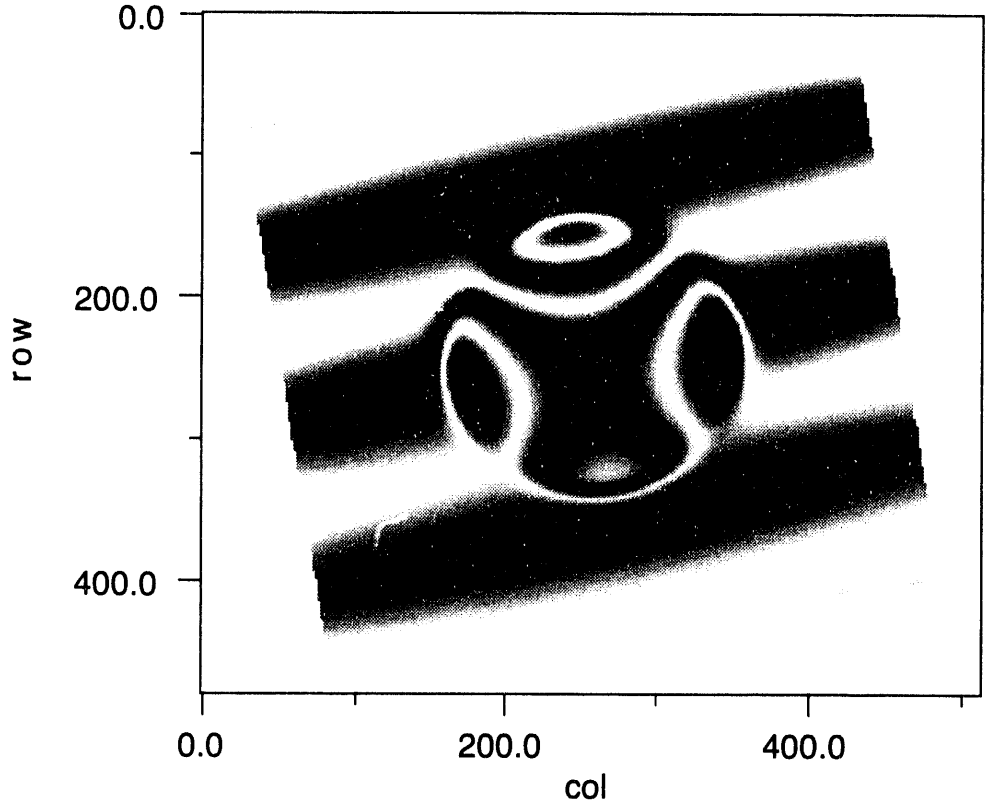

Figure 2: Typical Noise Free Raw Fringe Data Pattern for Noise Free Data

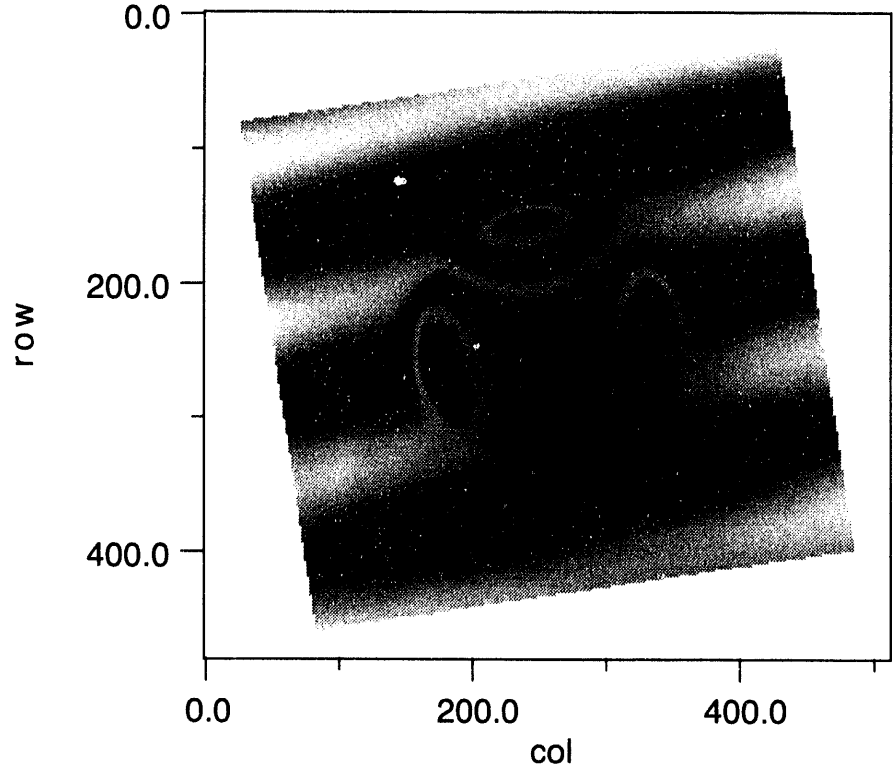

Figure 3: Synthetic Fringe Pattern: Noise Level = 2

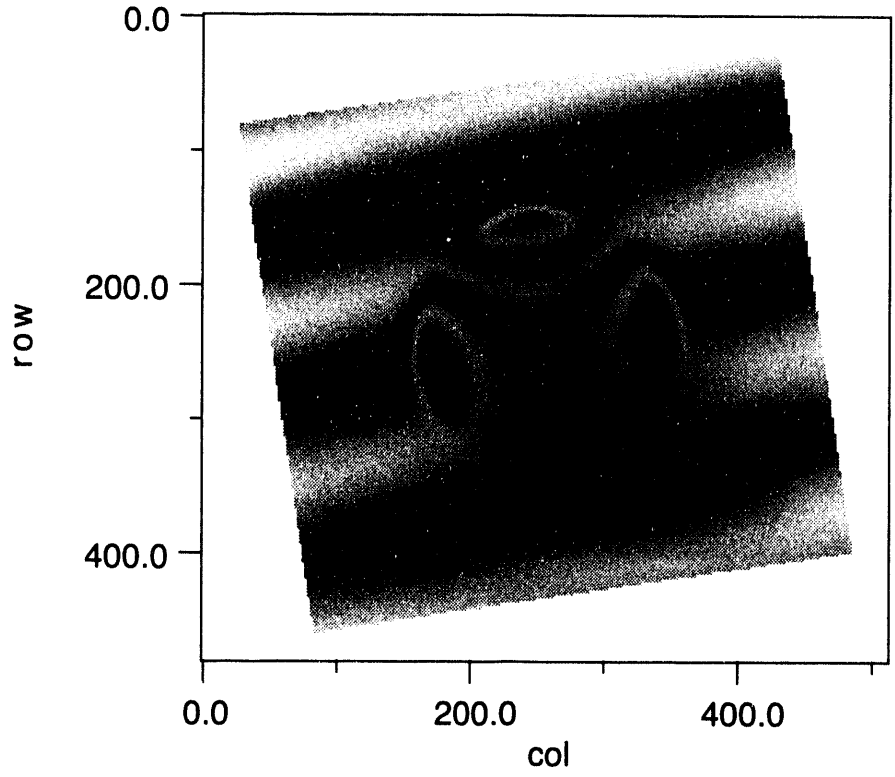

Figure 4: Synthetic Fringe Pattern: Noise Level = 5

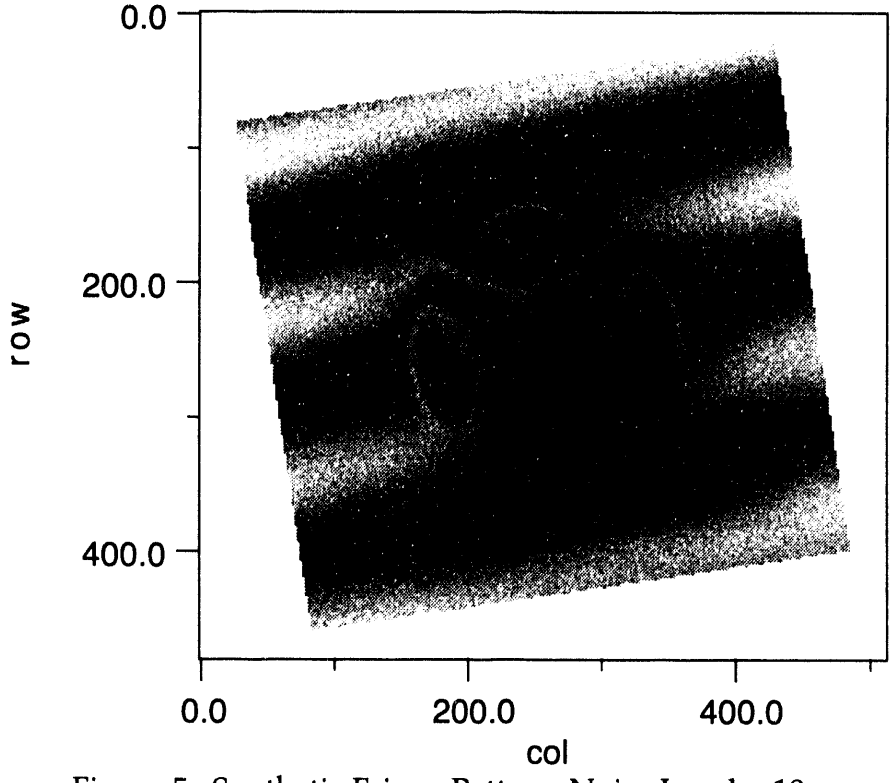

Figure 5: Synthetic Fringe Pattern: Noise Level = 10

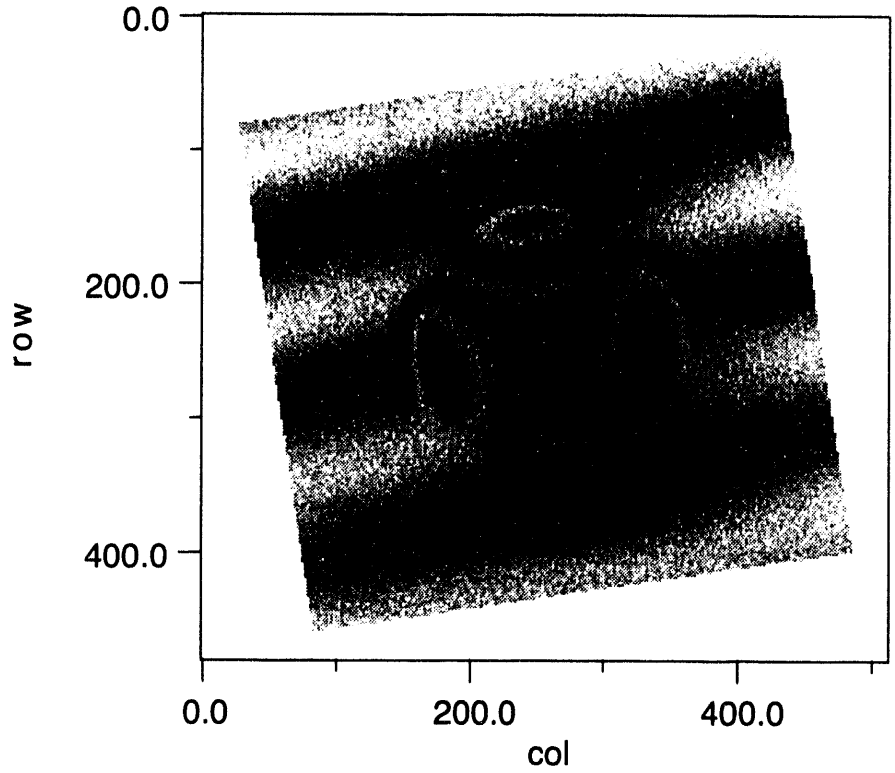

Figure 6: Synthetic Fringe Pattern: Noise Level = 20

DATE
FILMED
5/27/94

END